Industrial Crops & Products 188 (2022) 115667

Contents lists available at ScienceDirect

Industrial Crops & Products

journal homepage: www.elsevier.com/locate/indcrop

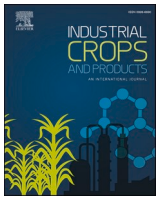

Association of cellulose micro/nanofibrils and silicates for cardboard coating: Technological aspects for packaging

Adriano Reis Prazeres Mascarenhas [a,*,1], Mário Vanoli Scatolino [b,e,2], Matheus Cordazzo Dias [c,3], Maria Alice Martins [d,4], Rafael Rodolfo de Melo [e,5], Maressa Carvalho Mendonça [c,6], Gustavo Henrique Denzin Tonoli [c,7]

[a] Department of Forest Engineering, Federal University of Rondônia (UNIR), 76940-000 Rolim de Moura, RO, Brazil
[b] Department of Production Engineering, State University of Amapá (UEAP), 68900-070 Macapá, AP, Brazil
[c] Department of Forest Science, Federal University of Lavras (UFLA), C.P. 3037, 37200-900 Lavras, MG, Brazil
[d] Embrapa Instrumentation, National Laboratory of Nanotechnology for Agribusiness, 13561-206 São Carlos, SP, Brazil
[e] Agricultural Sciences Center, Federal University of the Semiarid (UFERSA), 59625-900 Mossoró, RN, Brazil

ARTICLE INFO

Keywords:
Biopolymers
Multilayer packaging
Barrier properties
Surface energy
Tensile strength
Paper formability

ABSTRACT

Paper coating with cellulose micro/nanofibrils (MFC/NFC) can improve the performance of paper packaging. However, the process cost is high due to the significant energy consumption. The objective of this work was to produce MFC/NFC with pre-treated fibers using calcium silicate (Ca_2O_4Si) and magnesium silicate (MgO_3Si) and evaluate their performance as a coating on cardboard. For the production of MFC/NFC, pre-treatments with Ca_2O_4Si and MgO_3Si reduced energy consumption by ~30 %. The layers added to the cardboard reduced the water vapor permeability, mainly for the coating with 5 % MgO_3Si (~98 g mm/kPa^{-1}day m^2). These characteristics indicate that coated paperboard is suitable for packaging bread, cheese, fruit, and vegetables. Suspensions with 5 % and 10 % Ca_2O_4Si increased the spread of PVAc, PVOH, and printing ink. The coatings reduced the strength and stiffness of the papers by ~50 % compared to the uncoated paper due to the wetting and drying cycles. On the other hand, there was an increase in ductility, which potentiated the paper's formability. Optimizing application and drying techniques for MFC/NFC and silicate coating formulations can improve the mechanical and barrier properties of the coated papers for multilayer packaging.

1. Introduction

To ensure that packaging shows suitable properties to preserve the characteristics of the products, the industry combines paper with metals and petroleum-based polymers (Otto et al., 2021). However, these materials have considerable degradation time, and their accumulation in the environment risks human health and the life cycle in aquatic and terrestrial ecosystems (Mascarenhas et al., 2022a). It is estimated that around 30 % of the packages produced are single-use, mainly composed of non-biodegradable materials (Miller, 2020; Dey et al., 2021). Due to this, biopolymers have been extensively researched in renewable packaging production. Cellulose micro/nanofibrils (MFC/NFC) stand out in this context because they are renewable and have technological advantages. It can be used in packaging paper coatings, such as high

* Corresponding author.
E-mail addresses: adriano.mascarenhas@unir.br (A.R.P. Mascarenhas), mario_paraiso@hotmail.com (M.V. Scatolino), matheus.cordasso@gmail.com (M.C. Dias), maria-alice.martins@embrapa.br (M.A. Martins), rafael.melo@ufersa.edu.br (R.R. Melo), maressacmendonca@gmail.com (M.C. Mendonça), gustavotonoli@ufla.br (G.H.D. Tonoli).
[1] ORCID: 0000-0002-7554-3590
[2] ORCID: 0000-0002-0412-994X
[3] ORCID: 0000-0002-8154-2543
[4] ORCID: 0000-0002-6416-6929
[5] ORCID: 0000-0001-6846-2496
[6] ORCID: 0000-0001-7532-7794
[7] ORCID: 0000-0002-6502-8974

https://doi.org/10.1016/j.indcrop.2022.115667
Received 11 June 2022; Received in revised form 15 August 2022; Accepted 12 September 2022
Available online 22 September 2022

contact surface, biodegradability, high tensile strength, and the possibility of obtaining films/composites with a barrier to gases and fats (Mirmehdi et al., 2018a; Yu et al., 2019; Lu et al., 2022).

On the other hand, obtaining MFC/NFC demands high energy consumption to deconstruct the cell wall, therefore chemical or enzymatic pre-treatments are applied to the cellulosic pulp to facilitate the mechanical fibrillation process and obtain more individualized MFC/NFC (Cruz et al., 2022). One of the best-known pretreatments with high efficiency to facilitate fiber deconstruction is 2,2,6,6-tetramethylpiperidine-1-oxyl (TEMPO)-mediated oxidation, but the reagent cost is very high and can generate non-eco-friendly compounds, making it necessary to implement means of effluent recovery and treatment (Rol et al., 2019; Chen et al., 2022a).

This demonstrates the need for the development of new types of pretreatments that can provide individualization of NFC, lower energy consumption, and lower costs. Khadraoui et al. (2022) studied the production of NFC from marine lignocellulosic biomass and observed that combination of steam explosion and twin-screw extrusion associated with pretreatment with NaOH at concentrations of 10 or 20 % (w/w) allowed to obtain NFC with lower lignin contents and interesting characteristics for papermaking and biocomposites. Mnasri et al. (2022) employed different deep eutectic solvents for refining *Eucalyptus* and cotton fibers and observed modifications in crystallinity and xylan content. This resulted in increased water retention in the fibers and enhanced internal and external fibrillation of the cell wall. These authors also observed that the fibers obtained allowed the production of papers with superior mechanical properties, due to the increased amount of bonds and maintenance of fiber length.

Another option to reduce reagent costs is the use of alkaline treatments with NaOH or KOH, these reagents can be used because they can increase fiber swelling and reduce shear forces against the cell wall during fibrillation in ultra-refiners (Ang et al., 2019; Scatolino et al., 2022). Dias et al. (2019) produced NFC from *Eucalyptus* and *Pinus* fibers in ultra-refiners and found that the use of NaOH solutions at concentration of 5 % (w/w) under the temperature of 80 °C provided energy consumption reduction of around 40–60 %. Moreover, for *Eucalyptus* and *Pinus* fibers, Mascarenhas et al. (2022b) used alkaline solutions of sodium silicate (Na_2SiO_3) at concentrations of 5 % and 10 % (w/w) and observed improvements in the individualization of MFC/NFC and reduction of energy consumption during mechanical fibrillation in the order of ~50 % compared to untreated fibers.

The pretreatments can also be used to modify the cellulose surface, aiming to change the physical, chemical, optical, mechanical, and surface properties of MFC/NFC to broaden their range of applications (Rol et al., 2019). The modification of MFC/NFC for the production or coating of packaging papers has been addressed in many research. This is justified due to the improvements that the MFC/NFC provide in physical, mechanical, and barrier properties to water vapor, gases, and grease (Jin et al., 2021; Morais et al., 2021). To achieve these results, polymers and mineral additives can be added to MFC/NFCs, such as latexes, silanes, and nanoclays (Adibi et al., 2022; Oliveira et al., 2022; Saedi et al., 2021a).

The use of calcium silicate (Ca_2O_4Si) and magnesium silicate (MgO_3Si) solutions can be considered for this purpose, as they have a high pH (10−13) and can facilitate swelling, and promote swelling of the fiber cell wall, enhancing mechanical fibrillation. Research reports that these silicates have a high affinity for cellulose, which indicates the possibility of obtaining modified MFC/NFC (Liu et al., 2019; Zhang et al., 2018a). Nonetheless, few studies explore the possibility of using these silicates as pre-treatments for producing MFC/NFC aiming for their application in paper coatings for packaging production. Regarding this gap in scientific knowledge, the objective of the present work was to produce MFC/NFC from fibers pre-treated with calcium silicate and magnesium silicate and to evaluate its performance as a cardboard coating regarding microstructure, water absorption, and surface properties concerning water, adhesives and printing ink, barrier and mechanical properties.

2. Material and methods

2.1. Pre-treatment of the fibers

Bleached commercial Kraft pulp from *Eucalyptus* sp. (EUC), containing 79 ± 0.3 % of cellulose, 16 ± 0.1 % of hemicelluloses, and 0.4 ± 0.1 % of lignin was used in the study. The pulp was pre-treated with calcium silicate (Ca_2O_4Si), composed of 25 % CaO and 75 % SiO_2. A pretreatment with magnesium silicate (MgO_3Si) was also carried out, composed of 64 % of SiO_2 and 32 % of MgO. The silicates were provided by Dinâmica Química LTDA (São Paulo, Brazil). The calcium and magnesium silicate solutions were prepared with deionized water at concentrations of 5 % and 10 % (w/w). The EUC fibers were added to the solutions for the obtainment of suspensions with a concentration of 2.5 % (w/w). The suspensions were kept at a temperature of 80 ± 2 °C and constant stirring at 600 rpm for 2 h (Dias et al., 2019). Posteriorly, the treated pulps were washed in deionized water until reaching pH 7, in order to stop the reaction and avoid excessive fiber degradation. As a control, suspensions were produced with untreated EUC fibers in deionized water in a proportion of 2.5 %.

2.2. Production of the MFC/NFC

Pulps suspensions with and without pre-treatments were adjusted to concentrations of 2 % (w/w). The material was stirred for 15 min at 600 rpm to ensure dissociation and fiber swelling. The fibers were processed using a Masuko Sangyo MKGA-80 Supermasscolloider grinder (Kawaguchi, Japan) equipped with a rotating and static stone disc. The suspension was processed with five passes through the equipment at 1500 rpm (Mendonça et al., 2022). The distance between the stones was gradually modulated from 10 μm to 100 μm as the suspension viscosity increased.

In addition to the general suspension characteristics, to give a clear idea about the proportional amount of added additive mineral compound (Ca_2SiO_4 and or MgO_3Si), the authors performed the incineration of the MFC/NFC in a muffle furnace at 525 °C and calculated the residual silicate contents by discounting the average ash content of the untreated samples (Table 1). This characterization was performed using five repetitions employing the TAPPI T 211 om-02 (TAPPI, 2002) standard. (Table 2).

2.3. * Standard deviation; ** non-detected

The energy consumption was evaluated during the fibrillation process by considering the average electric current of each passage, the equipment voltage, the fibrillation time, and the initial mass of the untreated and pretreated pulps. The energy consumption was calculated for the passage in which the suspension presented gel consistency, ac-

Table 1
Parameters of MFC/NFC suspensions produced for cardboard coating.

Formulation	Viscosity (cP)	pH	MFC/NFC content	Silicate content	Solids content
			(%)	(%)	(%)
Control	7323 ± 173 *	7.2 ± 0.2	1.40 ± 0.05	ND* *	1.40 ± 0.05
Ca_2O_4Si 5 %	2853 ± 61	7.8 ± 0.2	1.20 ± 0.30	1.64 ± 0.40	2.85 ± 0.07
Ca_2O_4Si 10 %	4909 ± 142	7.0 ± 0.4	1.05 ± 0.08	2.99 ± 0.12	4.00 ± 0.20
MgO_3Si 5 %	2606 ± 50	7.7 ± 0.5	1.30 ± 0.04	1.47 ± 0.06	2.77 ± 0.10
MgO_3Si 10 %	3166 ± 152	7.1 ± 0.2	1.14 ± 0.06	2.30 ± 0.09	3.50 ± 0.15

Table 2
Characteristics of the coated cardboard with different formulations.

Types of coating	Coating thickness (μm)	Grammage (g/m^2)	Identification
Control paper (uncoated)	–	301 ± 1.5	*CP*
Wet control paper	–	302 ± 2.5	*WCP*
MFC/NFC	38.0 ± 3.0	313 ± 1.5	*MFC/NFC*
MFC/NFC pre-treated with Ca_2O_4Si 5 %	40.0 ± 3.6	312 ± 2.2	*CS 5 %*
MFC/NFC pre-treated with Ca_2O_4Si 10 %	39.0 ± 4.3	311 ± 2.0	*CS 10 %*
MFC/NFC pre-treated with MgO_3Si 5 %	40.8 ± 1.8	311 ± 2.6	*MS 5 %*
MFC/NFC pre-treated with MgO_3Si 10 %	38.0 ± 3.3	312 ± 1.4	*MS 10 %*

* Standard deviation

cording to Eq. 1.

$$EC \quad (kWh/t) = \frac{(P \times t)}{m} \tag{1}$$

Where P (voltage × electrical current) is the equipment potency (kW); t is the time spent for fibrillation (h); and m is the mass of pulp subjected to fibrillation (t).

2.4. Cardboard coating with MFC/NFC

Before applying the coatings, the suspension concentrations were adjusted to approximately 1.0 % (w/w), according to the solids content of MFC/NFC. A duplex commercial cardboard was used with a thickness of 0.48 ± 0.02 mm, a grammage of ~300 g/m^2, and dimensions of 297 × 210 mm. Four layers of the coating were applied to add a grammage of 12 ± 2 g/m^2 to the cardboard. A laboratory coating machine equipped with cylindrical bars with grooves for spreading the liquid was used to apply the suspensions to the paper surface at a 7 m/min speed. Three coats were applied with the grooved bar spaced at 0.5 mm, being the last layer applied with the bar without grooves. For each layer added, the paper was subjected to drying in an oven at 105 ± 2 °C for 10 min (Fig. 1).

Cardboard coated only with MFC/NFC without silicates, and uncoated papers were also evaluated. For evaluating the effect of wetting, the cardboards were wetted in a coating machine and subjected to drying, as well as performed for papers coated with several formulations (Fig. 2). For each treatment, five samples were evaluated.

2.5. Characterization of the fibers

2.5.1. Fourier transform infrared spectroscopy

Infrared vibrational spectroscopy analyzes were performed on the pulps pre-treated with silicate and untreated pulps A Varian 600-IR FTIR spectrometer with Fourier transform (FTIR) was used coupled with a GladiATR accessory from Pike Technologies (Santa Clara, USA). The measurements were done by attenuated total reflectance (ATR), at 45° with zinc selenide crystal. The spectral range was analyzed at 400–4000 cm^{-1}, resolution of 2 cm^{-1}, and 32 scans.

2.5.2. Water retention index

The water retention index (WRI) was determined based on the Scan C 62:00 standard (SCAN, 2000). Suspensions containing 0.5 % (w/w) of treated and untreated fibers were prepared. Subsequently, the water from the suspension was drained in a Thermo Fisher Scientific Heraeus Megafuge 16 R centrifuge (Waltham, USA), and adjusted to a force of 3000 G for 15 min. The fibers retained on the sieve were weighed and subjected to drying at a temperature of 100 ± 2 °C until a constant mass. This assay was performed with four repetitions for each pretreatment and the WRI was calculated according to Eq. 2.

$$WRI \quad (g/g) = \left(\frac{M_1}{M_2}\right) - 1 \tag{2}$$

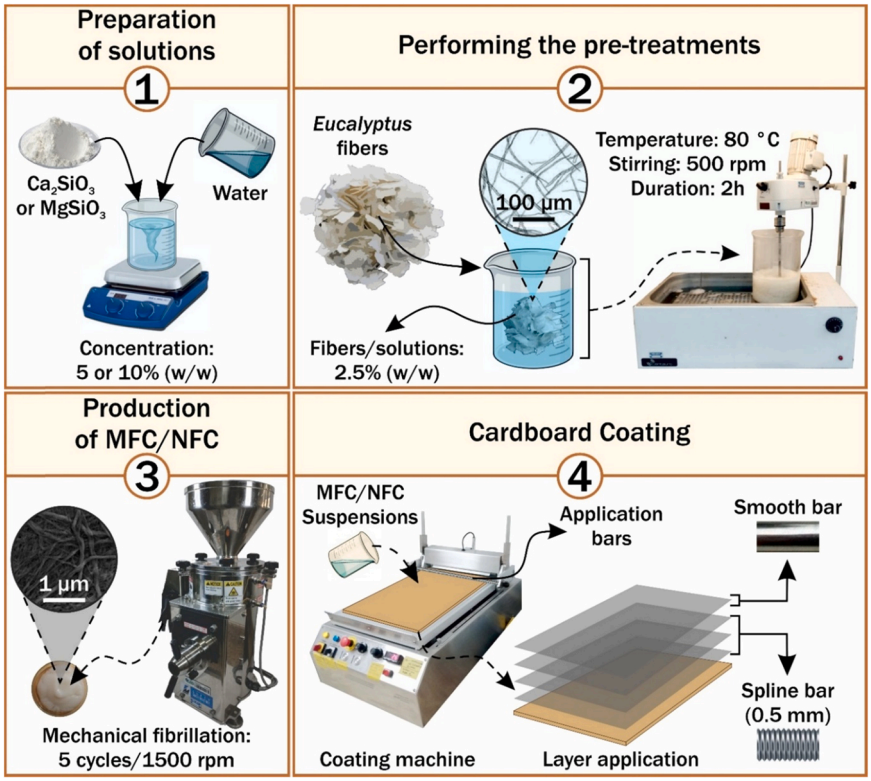

Fig. 1. Scheme of pre-treatments with calcium silicate and magnesium silicate on the EUC fibers; production of MFC/NFC, and cardboard coating.

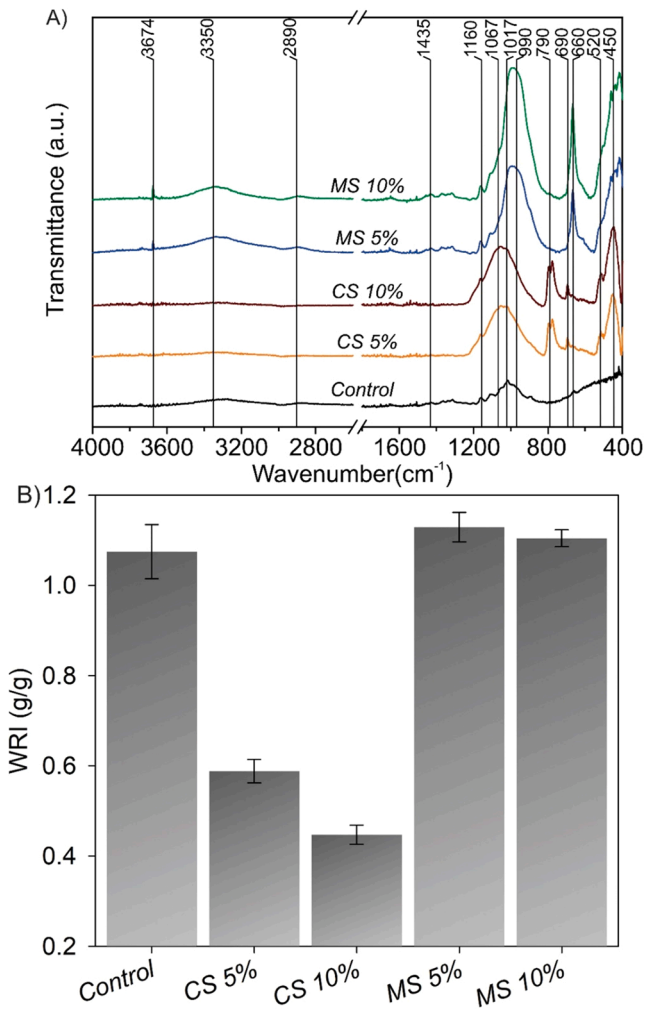

Fig. 2. A) Typical FTIR spectra and B) WRI for untreated and pre-treated fibers with silicates.

Where M_1 and M_2 are the masses after draining in a centrifuge and after drying, respectively.

2.6. Characterization of the MFC/NFC suspensions

2.6.1. Microstructural analysis of MFC/NFC

For analysis of the particles in the suspensions after the fibrillation process, images were obtained by an Olympus BX41 light microscope (Tokyo, Japan). The MFC/NFC suspensions were diluted in deionized water to a concentration of 0.10 % (w/w). Drops of MFC/NFC suspensions were added to glass slides, which were covered with a coverslip for observation using an objective of 10x at a range of 1280 × 1024 pixels.

In addition, samples of the suspensions at a concentration of 0.001 % (w/w) MFC/NFC were sonicated at 150 Hz for 2 min (Silva et al., 2020). Subsequently, small aliquots were added to the double-sided carbon tape adhered to the aluminum sample holder (stubs). After an overnight period in a desiccator with silica gel, the samples were gold metalized in a sputtering device (SCD 050). The morphology of the MFC/NFC was observed on an ultra-high resolution (UHR) field emission scanning electron microscope (SEM/FEG) TESCAN CLARA (Libušina, Czech Republic) using 10 KeV, 90 pA and 10 mm working distance. MFC/NFC diameters were measured for at least 200 individual structures using ImageJ software (Rueden et al., 2017).

2.6.2. Stability and zeta potential of the suspensions

The suspension stability test was conducted according to the methodology presented in Guimarães Júnior et al. (2015). MFC/NFC suspensions (10 mL) with a concentration of 0.25 % (w/w) were previously homogenized in a magnetic stirrer at 500 rpm for 1 h and poured into tubes. For each pre-treatment, five samples of the suspensions were photographed every 1 h for a total period of 8 h. The software ImageJ (Rueden et al., 2017) was used to measure the total height of the liquid and the height of the suspended MFC/NFC of each image. The stability was calculated according to Eq. 3.

$$Stability \quad (\%) = \left(\frac{S}{T}\right) \text{x} 100 \tag{3}$$

Where S corresponds to the height of the suspended particles in the tube, and T corresponds to the total height of the liquid present in the tube.

The zeta potential (ζ) was determined in order to evaluate the effect of pre-treatments on the electrostatic stability of MFC/NFC suspensions. The Nano-ZS90X Malvern Zetasizer equipment (England, United Kingdom) was turned on for 30 min, for calibration, before the measurements. The readings were performed at a temperature of 25 °C, using 1 mL of each coating formulation with a concentration of 0.1 % (w/w). Five measurements were performed for each treatment (Zhang et al., 2018a).

2.6.3. X-ray diffraction (XRD) of MFC/NFC

X-ray diffraction (XRD) was performed to verify possible changes in the crystalline structure of the cellulose after the pre-treatments were performed. Spectra were acquired from intact films produced from MFC/CNF by the "casting" method. The analyzes were performed using an x-ray diffractometer Shimadzu Corporation XRD 6000 (Kyoto, Japan), adjusted with Cu Kα radiation (1.1540 Å) at 30 kV and 30 mA. Scattered rays were collected in the range of 2θ = 10–40º, a rate of 2 °/min (Tonoli et al., 2021). Curve noises were removed by the adjacent average method, with 10 points per window, producing smoothed patterns without compromising peak information.

2.7. Characterization of the coated papers

2.7.1. Microstructural analysis of the papers

Samples with 5 × 5 mm of the coated and uncoated papers were submerged in liquid nitrogen for flash freezing, fractured with a scalpel, and fixed on sample holders (stubs) containing double-sided carbon adhesive tapes. Subsequently, the material was subjected to metallic coating in a gold evaporator (SCD 050) and analyzed in a scanning electron microscope with field emission (SEM/FEG) TESCAN CLARA (Libušina, Czech Republic), with ultra-high resolution (UHR), under conditions of 10 KeV, 90 pA, and a working distance of 10 mm. Micrographs of the fracture and the top of the cardboard samples were obtained. The energy dispersive spectroscopy (EDS) analysis was performed to evaluate the penetration of the coatings in the cardboard. The X-Flash6–60 Bruker X-ray detector (Billerica, USA) from the SEM/FEG was calibrated for the element analysis condition. The SEM with EDS with 500x magnification allowed the obtainment of energy spectra of the elements along with the fracture profile (line scan mode). The elements distribution (mapping function) along the samples was studied with a working distance close to 10 mm, Kcps value greater than 30 units, voltage at 20 KeV, and Bean Current around 5 ηA.

2.7.2. Contact angle, wettability, and free surface energy

The contact angle and wettability of the cardboards were evaluated according to the TAPPI T 458 cm-14 (TAPPI, 2014). The measurements of the contact angle were performed using a Krüss DSA30 goniometer (Hamburg, Germany). Ten samples with dimensions of 10 × 50 mm were cut, which were fixed on a glass slide. For evaluation, 15 μL of deionized water was dripped on the papers to calculate the average contact angle between the water drop and the surface after 1 s. The wettability of the papers was calculated with the average values of the

contact angles measured between 5 and 55 s, according to Eq. 4.

$$Wettability \quad (^{\circ}/s) = \frac{(A-a)}{55} \tag{4}$$

Where A is the average contact angle after 5 s (°) and a is the average contact angle after 60 s (°).

To verify the ability to spread adhesives on the surface of coated cardboards, the test was also conducted using polyvinyl acetate - PVAc for industrial use. To evaluate the coated papers as a spreading agent for other industrial coatings, the contact angle and wettability were evaluated for polyvinyl alcohol (PVOH) diluted in deionized water at a concentration of 5 % (w/w) with the agitation of 300 rpm at 90 °C, produced by Kuraray America Inc. (Texas, USA). The spread of ink on the cardboard surface was also evaluated, using the T504 printing ink produced by Epson Brazil Ind. LTDA (São Paulo, Brazil). These tests were performed using 20 samples and adapting some procedures from ASTM D7490–13 (ASTM Standard, 2022). The surface free energy was obtained according to the methodologies presented by Tonoli et al. (2009) and Arantes et al. (2019) using the same goniometer abovementioned. The liquids used for the test are shown in Table 3.

2.7.3. Water absorption (Cobb test)

The water absorption test (Cobb Test) was performed according to ASTM D3285–93 (ASTM Standard, 2005). Five samples with dimensions 125 × 125 mm were cut and kept in a desiccator with silica for 72 h at room temperature (25 ± 2 °C), and weighed. The papers were fixed in a Cobb Tester TKB Instruments (São Paulo, Brazil) and 100 mL of deionized water was poured into the equipment ring that delimits a certain area of the paper surface, for 2 min. The excess water was removed from the paper surface. The paper was placed between two sheets of blotting paper and pressed with a cylindrical roller. Finally, the papers were weighed again to calculate the water absorption by Eq. 5.

$$Cobb \quad (g/m^2) = (M_i - M_f) \times 100 \tag{5}$$

Where *Mi* and *Mf* are the mass (g) of the paper, before and after the contact with water, respectively.

2.7.4. Water vapor permeability

For each treatment, five circular samples with a diameter of 16 mm were prepared. The samples were stored in an air-conditioned room with a temperature of 25 °C and relative humidity of 65 % for 3 days, according to ASTM E96–16 (ASTM Standard, 2016a). The samples were placed in glass capsules partially filled with s í lica previously dried at 105 °C, which were placed in desiccators containing a saturated solution of KCℓ at 38 °C to obtain an atmosphere with a relative humidity of 90 %, according to ASTM E104–02 (ASTM Standard, 2012). The capsules with the papers and silica were weighed on an analytical balance for 8 days. The water vapor transmission rate (WVTR) and water vapor permeability (WVP) were calculated using Eq. 6 and Eq. 7.

$$WVTR \quad (g/m^2 day) = \frac{w}{t \times A} \tag{6}$$

$$WVP \quad (g \ mm / kPa^{-1} day \ m^2) = \frac{(WVTR \times e)}{(p \times UR_f - UR_d)} \tag{7}$$

Table 3
Characteristics of liquids used for surface free energy test.

Test liquids	Superficial tension (mJ/m²)		
	Dispersive	Polar	Total
1-Bromo-2-naphthalene	44.6	0	44.6
Ethylene glycol	29.0	19.0	48.0
Di-iodomethane	48.5	2.3	50.8
Glycerol	37.0	26.4	63.4
Water	21.8	51.0	72.8

Where w is the mass of the capsule with sample (g); t is the time (days); A is the exposed area of the sample (m^2); e is the sample thickness (mm); p is the water vapor pressure (kPa) and URf - URd is the difference between the humidity outside and inside the capsule at 38 °C.

2.7.5. Mechanical characterization of the papers

The mechanical tests were performed with an adaptation of the ASTM D 828–16e1 (ASTM Standard, 2016b). The Stable Micro Systems TATX2i texturometer (Godalming, United Kingdom) equipped with a 500 N load cell was used to determine the strength, Young's modulus, and elongation at break in the tensile test. Ten specimens with dimensions of 10 × 100 mm were tested with an initial distance of 50 mm between the grips and a test speed of 0.8 mm/s.

2.8. Statistical analysis

Data were analyzed using graphic analysis (FTIR and XRD) and descriptive statistics, sketching column graphs with the averages and standard deviation for each property.

3. Results and discussion

3.1. FTIR and WRI

From the spectral curves of the pre-treated pulps, it was possible to observe the presence of peaks referring to the functional silicate groups, even after washing and stabilization of the pH. For *CS 5 %* and *CS 10 %*, there was a significant reduction in the angular vibration peaks of the C-H and -OH cellulose groups (Fig. 2), situated around 2890 and 3350 cm^{-1} (Lopes et al., 2018), indicating a strong interaction of the calcium silicate with the fibers. This behavior was also observed by Li et al. (2010) when studying the synthesis of cellulose and calcium silicate composites using ethanol in their solubilization.

To obtain similar results, Li et al. (2018) used hydrochloric acid to facilitate solubilization and exposure of calcium silicate fillers to enhance its interaction with cellulose. From the point of view of industrial scaling, these results highlight the advantages of the process carried out in the present work, because it was not necessary to use additional reagents to increase the impregnation of calcium silicate to cellulose, making the fibers pre-treatment cheaper and more eco-friendly. Another evidence that shows the modification of the fibers pre-treated with calcium silicate is the absorption range between 448 and 457 cm^{-1}, which corresponds to the angular vibration of SiO_4, and tetrahedral Si-O-Si (Ray et al., 2018; Rotermel et al., 2021). Peaks observed in the range from 980 to 990 cm^{-1} correspond to the stretching of the Si-O, Si-O-Ca, and O-Si-O vibrational modes (Puertas et al., 2004; Li et al., 2010). The increase in peak intensity in the bands 690 and 790 cm^{-1} correspond to the absorptions of Si-O-Si and SiO bonds, respectively (Al-Oweini e El-Rassy, 2009, Gupta et al., 2019).

Fiber modification was also observed when using magnesium silicate, which can be occurred due to the increase in intensity in the band of 473 cm^{-1} and in the absorption bands situated between 540 and 660 cm^{-1}, which correspond to the stretching of the vibrational mode of Mg-O (Selvam et al., 2011; Jeevanandam et al., 2013). An increase in absorption intensity was also observed between the bands of 1420 and 1481 cm^{-1}, corresponding to Mg-OH (Hofmeister and Bowey, 2006). Another point that indicates the fiber modification with magnesium silicate is the peak located around 3674 cm^{-1}, attributed to the -OH group of magnesium ions, located in the octahedral sheets of the mineral (Frost e Mendelovici, 2006). Regarding the peaks referring to the angular vibration of the C-O and C-O-C cellulose bonds (1017 cm^{-1} ~ 1160 cm^{-1}) (Foster et al., 2018; Khan et al., 2020), they were not clearly identified in the fibers pre-treated with magnesium silicate. This occurred because there was an increase in the peak intensity located at 1088, 801, and 456 cm^{-1}, which are attributed to asymmetric

stretching, symmetrical stretching, and vibration bending of the Si-O-Si bonds, respectively (Zhu et al., 2017). Another possibility that explains the absence of peaks for C-O, is also related to the overlapping of the asymmetric vibration of O-Si-O located around 1097 cm^{-1} (Jia et al., 2011). The behavior was also observed for fibers pre-treated with calcium silicate. It was also observed in the pre-treated fibers, the suppression of the peak intensity situated between 810 and 896 cm^{-1}. This spectral region corresponds to the angular vibration of the C-OH groups of the β-glycosidic bonds that bind hemicelluloses to cellulose (Ikramullah et al., 2017; Özgenç et al., 2017). The changes can directly influence the surface loads of the cellulose, which affect the interaction with water and physical and colloidal properties.

The greatest reductions in water retention index (WRI) were observed for the fibers pre-treated with calcium silicate. The WRI of the *CS 5 %* and *CS 10 %* were, respectively, 45 % and 58 % lower compared to the control (~1.1 g/g) (see Fig. 2B). These reductions can be explained by the interaction of the silicate with the -OH cellulose groups. Chen et al. (2019) and Meija-Ballesteros et al. (2021) explained that this effect increases the velocity of capillary water flow out of the cell walls due to the reduction in the number of hydrogen bonds between water and cellulose, reducing the fiber WRI. The fibers pre-treated with magnesium silicate presented a slight increase in the WRI. For *MS 5 %*, the increase concerning the control was around 5 % and ~2.8 % for *MS 10 %*. The increase in the WRI occurred due to the Mg-OH groups of the magnesium silicate and little influence on the reduction of the intensity for the -OH cellulose groups. Huan et al. (2018) observed that the addition of magnesium silicate to composites reinforced with carbon sheets resulted in increased porosity and water adsorption capacity.

Even so, the WRI values are in agreement with what has been observed in other works in the literature. Mnasri et al. (2022) verified in *Eucalyptbus* fibers WRI values ranging between 1 and 1.35 g/g after application of enzymatic and deep eutectic solvent pretreatments. Using the same pre-treatments, these authors found WRI values for cotton ranging from 0.6 and 0.8 g/g. Similarly, Mejia-Ballesteros et al. (2021) studied the effect of hornification on unbleached *Eucalyptus* fibers and obtained WRI values around 1.7 and 1.1 g/g for unhorned fibers and fibers submitted to four hornification cycles, respectively.

3.2. *Microstructural analysis, fibrillation energy consumption, stability, zeta potential, and XRD of the suspensions*

The untreated fibers resulted in MFC/NFC suspensions with cell wall fragments and bundles of partially joined fibrils (Fig. 3). Regarding the suspensions of *CS 5 %* and *CS 10 %* (Fig. 3D e 3G), it was possible to notice that fibrillation occurred more efficiently because the dimensions of the bundles and cell wall fragments were significantly smaller compared to the *Control* (see Fig. 3A and 3B). However, it was possible to observe the calcium silicate particles in both suspensions (see Fig. 3E e 3H).

The suspensions of *MS 5 %* and *MS 10 %* were more homogeneous

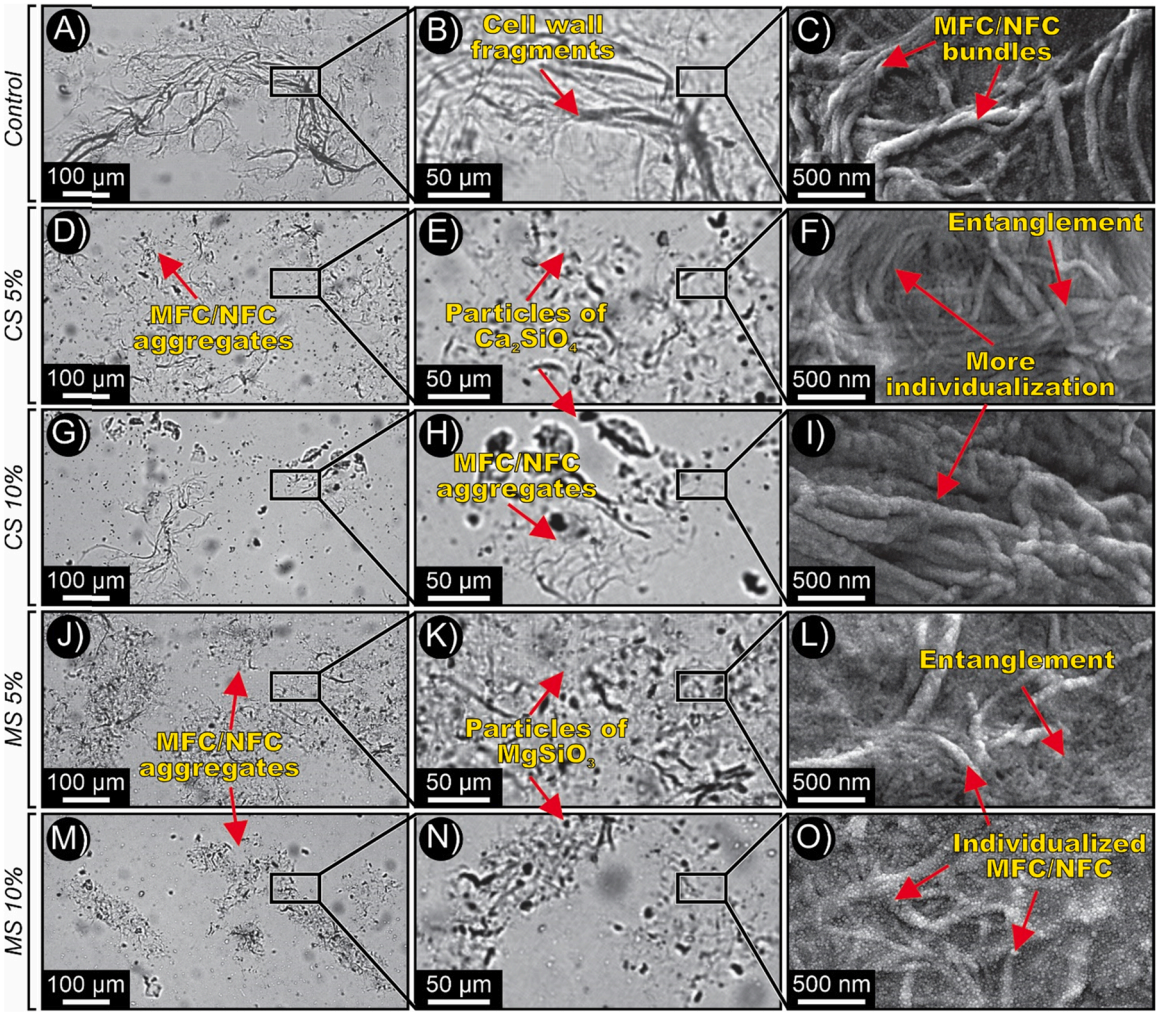

Fig. 3. Light microscopy and SEM images of the EUC MFC/NFC, untreated and pre-treated with calcium silicate and magnesium silicate solutions; A-C) Control; D-F) *CS 5 %*, G-I) *CS 10 %*; J-L) *MS 5 %*; M-O) *MS 10 %*.

among all, showing more cohesive clusters of MFC/NFC and smaller cell wall fragments (see Figs. 3J and 3M), which indicates a greater ability to deconstruct fibril bundles. In addition, the residual particles of magnesium silicate are smaller compared to calcium silicate (see Figs. 3K and 3N). To better understand the mentioned aspects, Fig. 4 shows the frequency distributions as a function of the diametric classes of the MFC/NFC obtained from the SEM images. For the *Control* (Fig. 3C), diameters of the MFC/NFC were obtained around ~58 nm. In addition, 68 % of the structures had diameters below 60 nm.

Regarding *CS 5 %* and *CS 10 %* (Figs. 3F and 3I), the average diameters of MFC/NFC were around ~42 nm and ~45 nm, respectively. Considering the frequency of diameters below 60 nm, around ~86 % of the structures observed for *CS 5 %* presented themselves in this condition and for CS 10 % the frequency was 90 %. The MFC/NFC from *MS 5 %* and *MS 10 %* had average diameters of ~46 nm and ~55 nm, respectively (Figs. 3L and 3O). In *MS 5 %*, around ~85 % of the structures showed diameters below 60 nm, while for *MS 10 %* the frequency of structures in this condition was ~66 %. These results indicate that silicate pretreatments improved fibrillation efficiency, especially when calcium silicate was used.

Despite the reduction in the WRI caused by the calcium silicate, which could hinder the MFC/NFC obtainment, the mechanical fibrillation may have been favored by the initial fiber swelling due to the high pH (10−13) during the pre-treatment. The cell wall swelling potentiates the shear against the grinder stones, increases the surface area of the three-dimensional MFC/NFC network during the dissociation of the fibril bundles, and promotes the "gel" obtainment with fewer passes (Gorur et al., 2020; Martins et al., 2021). The magnesium silicate (pH~10.5) promotes fiber swelling, and the presence of Mg-OH groups increases the water entry capacity between the cellulose fibrils (Dimic-Misic et al., 2013; Dias et al., 2019).

The energy consumption to obtain the MFC/NFC reinforces this reasoning. For the *Control*, around 8000 ± 308 kWh/t were required to obtain the gel. Considering the *CS 5 %* and *CS 10 %* pre-treatments, the energy consumption was around 6166 ± 94 kWh/t and 5833 ± 71 kWh/t, respectively. Concerning *MS 5 %* and *MS 10 %*, approximately 7000 ± 119 kWh/t and 5850 ± 58 kWh/t were needed to obtain gel, respectively. Both calcium silicate and magnesium silicate are insoluble in water, nonetheless, when dispersed in an aqueous medium, they have a great capacity for gel formation (Wang et al., 2019; Tang et al., 2021). Mascarenhas et al. (2022b), using sodium silicate solutions at concentrations of 5 % and 10 % (w/w), found energy consumption for fibrillation of *Eucalyptus* and *Pinus* bleached pulps in the range of 3000–4100 kWh/t and 4000–4500 kWh/t, respectively. Mendonça et al. (2022) studied alkaline pre-treatments with NaOH to facilitate mechanical fibrillation and found reductions in energy consumption of ~31 % for *Eucalyptus* and ~28 % for *Pinus*. In the present work, the reductions in energy consumption were on the order of ~22 % and ~27 % for *CS 5 %* and *CS 10 %*, respectively. For *MS 5 %* and *MS 10 %*, the reductions in energy consumption for fibrillation were ~12.5 % and ~27 %, respectively.

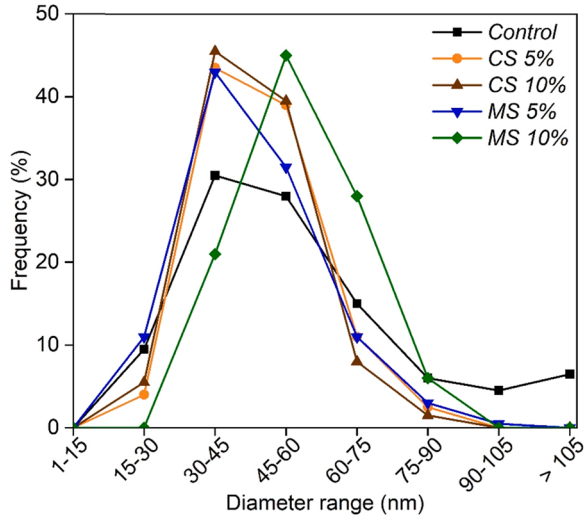

Fig. 4. Diametric distribution histograms showing the general occurrence of MFC/NFC for untreated and pre-treated with calcium silicate and magnesium silicate solutions.

These results are unprecedented and meet part of the objectives of this work. This demonstrates that the silicates, in addition to favoring individualization and increasing the MFC/NFC homogeneity, promoted a significant reduction in energy consumption, making the process more efficient. This effect was assumed to be due to the silicate alkalinity and also by the intensification of the shear of the fiber cell walls. The impregnation of the silicate particles on the fiber surfaces may have increased the abrasion of the cell walls with the grinder stones, which may explain the smaller dimensions of the fibril bundles and fragments in the suspensions.

Scatolino et al. (2022) explained that the alkaline pre-treatments in fibers contribute to the reduction of the hemicellulose content and increase fiber swelling. Furthermore, they can facilitate the MFC/NFC obtainment in the grinder with a reduction in energy consumption of more than 45 % during mechanical fibrillation (Ang et al., 2019). The results are interesting for applying these suspensions as a coating on the paper using bars and considering the possibility of industrial scaling. Particles with smaller dimensions allow an optimized distribution of the suspensions on the paper surface, reducing the appearance of discontinuities between the applied layers (Tyagi et al., 2021).

After 8 h, the stabilities of the *CS 5 %* and *CS 10 %* suspensions were 46 % and 70 % lower compared to the control (92 %), respectively (Fig. 5A).

Regarding *CS 5 %*, in the first 4 h of evaluation, the stability of the suspensions was abruptly reduced. From 5–8 h of testing, the sedimentation of MFC/NFC suspensions was small (2 %). For *CS 10 %*, the stability reduced by 2/3 of the original condition during the first 4 h of testing. From this moment to the end of the test, the variation was not notorious (~1.7 %). The *MS 5 %* suspension showed a reduction of the stability of around 22 % compared to the control. For the *MS 10 %* suspension, this reduction was around 57 %. *MS 5 %* showed no tendency to stabilize the sedimentation of the particles because the stability was reduced until the end of the test. On the other hand, the *MS 10 %* had its stability reduced by 2/3 after 6 h of testing. Posteriorly, the sedimentation was increased by ~4 %.

The reduction in the stability of suspensions obtained from fibers pre-treated with silicates is related to the impregnation of the -OH cellulose groups, which are the main ones responsible for the electrostatic repulsion of MFC/NFC in aqueous media (Li et al., 2021). This effect was more intense for calcium silicate. For magnesium silicate, as already demonstrated, the presence of Mg-OH groups may have contributed to the maintenance of particles in suspension. Calcium silicate and magnesium silicate are insoluble in water and have positive charges on their surfaces (Ca^{2+} and Mg^{2+}) besides different configurations of amorphous silica (Spinthaki et al., 2018; Tipper et al., 2021). This contributes to the impregnation of cellulose by silicates, interruption of the repulsion of charges in the water, and reduction of the dynamics of random movement of particles (Brownian movement), enhancing the sedimentation of MFC/NFC (Yang et al., 2021). Silva et al. (2021) also observed similar behavior when they submitted bleached *Eucalyptus* MFC to drying and redispersion cycles. These authors found that drying promoted the formation of MFC aggregates that limited the electrostatic repulsion capacity, which increased the sedimentation of the suspensions by ~50 %.

The results for the zeta potential of the suspensions reinforce the explanations presented (see Fig. 5B). The values for *CS 5 %* and *CS 10 %* were around − 25 and − 34 mV, which were 32 % and 76 % lower than the control, respectively. For *MS 5 %*, the results for ζ were around

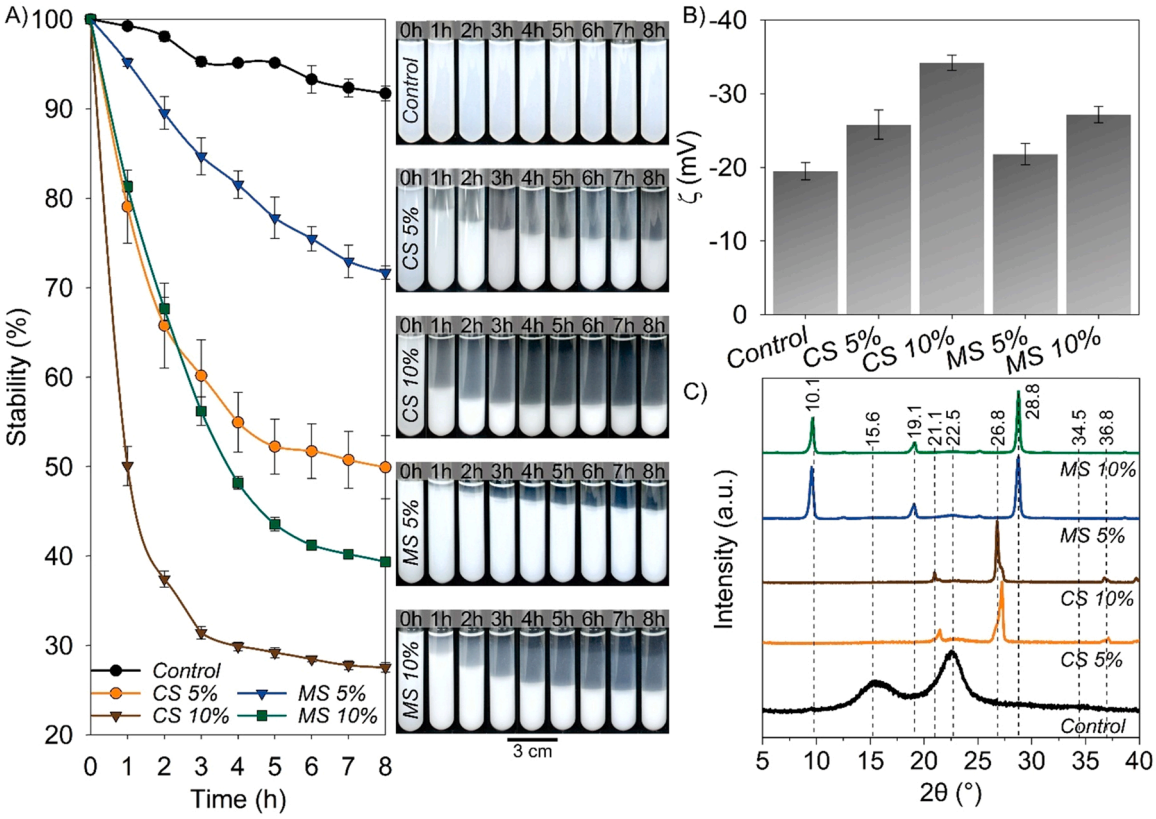

Fig. 5. A) Stability, B) zeta potential (ζ) C) x-ray diffractograms of EUC MFC/NFC suspensions untreated and pre-treated with calcium silicate and magnesium silicate solutions.

− 21 mV, being ~8 % lower compared to the control. For *MS 10 %*, the ζ values were around − 27 mV, which represented a 40 % of reduction in relation to the control. According to Patel and Agrawal (2011) and Bhattacharjee (2016), colloidal suspensions can be classified according to ζ as highly unstable (0 to −10 mV), relatively stable (± 10 to −20 mV), moderately stable (± 20 to −30 mV), and highly stable (> ± 30 mV). Blanco et al. (2018) showed that ζ values lower than − 15 mV indicate that MFC/NFC suspensions may show a tendency to agglomeration and sedimentation. In addition, suspensions with ζ values lower than 25 mV, or greater than − 25 mV may eventually agglomerate, due to interparticle interactions, including van der Waals forces and hydrogen bonds (Predoi et al., 2020). This behavior was also observed in the present work.

The stability of suspensions is one of the main technological variables involved in the context of paper coating (Pawlowski, 2009). Maintaining the viscosity of the formulations is essential for obtaining paper coatings with uniform surface and interlayer distribution (Liu et al., 2017). Shenoy and Shetty (2022) showed that ζ and surface tension are correlated. These authors found that clay-based suspensions with ζ values around − 30 mV resulted in increased surface free energy of the coating, improving fixation and transfer of ink onto cardboard.

These results can be explained by the modification of the crystalline pattern of the cellulose with the pre-treatments (Fig. 5C). In the sample referring to the *Control*, the diffraction peaks of halos located at 2θ = 14.9–16.5°, 22.5°, and 34.5° are clearly presented, attributed to the crystalline planes (1−10), (110), (200) and (004) of type I cellulose, respectively (French, 2014). When observing the diffractograms of *CS 5 %* and *CS 10 %* it is possible to notice that the intensity of the cellulose crystalline halos was suppressed due to the appearance of peaks located at 2θ = 21.1°, 26.8°, and 36.8° which are referring to the typical crystallographic pattern of Ca_2O_4Si and $Ca_2O_4Si\ {}_xH_2O$ (Meiszterics et al., 2010). Li et al. (2010) and Jia et al. (2011) obtained similar results to the present work and found that this effect is due to the strong interaction between calcium silicate and cellulose.

For *MS 5 %* and *MS 10 %*, the typical crystallographic pattern of cellulose I was also not identified. Classic diffraction peaks of MgO_3Si were observed with values of 2θ = 19–30° and 2θ = 32–38°, which were consistent with results obtained in the literature (Wang et al., 2010; Zhao et al., 2015). Between 2θ = 10° and 19.1° peaks referring to the presence of MgO_3 and $Mg(OH)_2$ were observed (Jin and Al-Tabbaa, 2013; Zhang et al., 2018b). High-intensity peaks located at 2θ = 28.8°, on the other hand, indicate the presence of residual silica from magnesium silicate (Darghouth et al., 2021), strongly adhered to cellulose. These results corroborate the behavior observed for stability and zeta potential, confirming the strong interaction of silicates even after the mechanical fibrillation process, proving the occurrence of modifications in the chemical structure of cellulose.

These aspects allow the predictability of the coating parameters (e.g. weight, gas barrier, strength) according to the purpose of the paper application (Tyagi et al., 2021; Jin et al., 2021). With the knowledge of viscosity and stability, it is possible to make decisions regarding the need to implement suspension agitation, speed of application, and the dimension of the amount of material to be prepared for use in the production line.

3.3. Microstructural analysis, contact angle, wettability, and surface energy of the papers

SEM micrographs allowed us to observe that the wetting and drying of the paper resulted in surface modification in relation to control paper (*CP*) (Fig. 6). It was possible to notice greater amounts of void spaces on the wet control paper (*WCP*) surface (Fig. 6D) due to the swelling and contraction of the fibers resulting from the adsorption and desorption of water (Hubbe et al., 2007). These modifications also occurred between

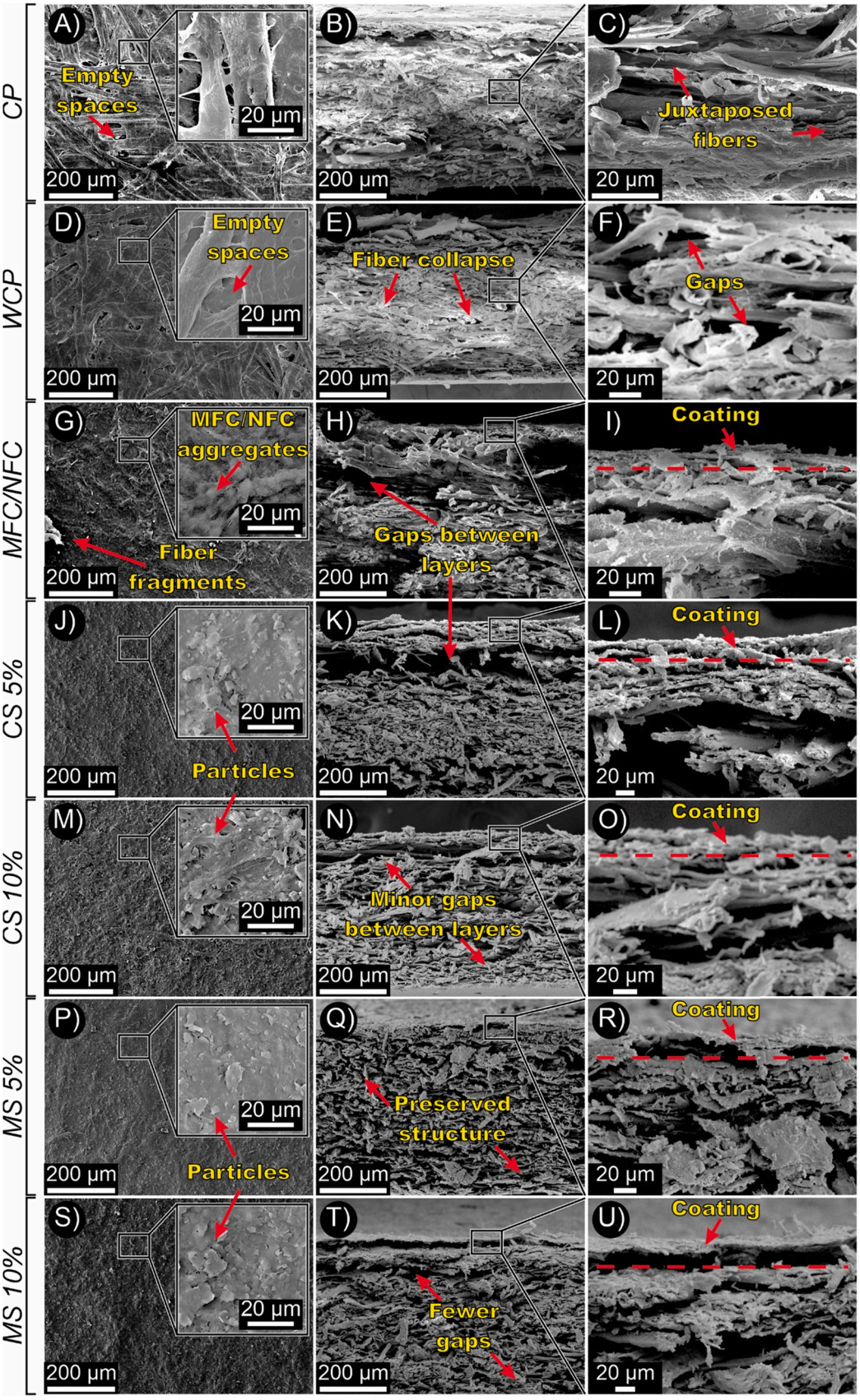

Fig. 6. SEM micrographs of the EUC MFC/NFC coated cardboard from *Eucalyptus* sp. untreated and pre-treated with calcium silicate and magnesium silicate solutions; A) *CP* surface; B) *CP* cross-section; and C) *CP* cross-section zoom; D) *WCP* surface; E) *WCP* cross-section; F) *WCP* cross-section zoom; G) MFC/NFC surface; H) MFC/NFC cross-section; I) MFC/NFC section zoom; J) *CS 5 %* surface; K) *CS 5 %* cross-section; L) *CS 5 %* cross-section zoom; M) *CS 10 %* surface; N) *CS 10 %* cross-section; O) *CS 10 %* cross-section zoom; P) *MS 5 %* surface; Q) *MS 5 %* cross-section; and R) MS 5 % cross-section zoom; S) *MS 10 %* surface; T) *MS 10 %* cross-section; and U) *MS 10 %* cross-section zoom.

the layers of the paperboard. Compared with *CP* (Figs. 6B and 6 C), in the *WCP* the cell walls collapsed and the fibers rearranged (Fig. 6E). This induced the formation of more gaps and micro galleries in relation to the original paper (Fig. 6 F). This effect was also described by Thébault et al. (2017) when presenting the main factors involved in the process of coating paper with phenolic resins. Regarding the coating with MFC/NFC, it was possible to observe that the irregularities and the number of voids on the paper surface were significantly reduced. However, fragments of the cell wall of the suspension were observed distributed on the paper surface (Fig. 6 G).

In the cross-section, voids were also formed between the layers of paperboard due to the effect of wetting and successive drying (Fig. 6H). Oliveira et al. (2022) explained that many cycles of wetting and drying during the application of the coatings cause the hornification of the fibers, inducing the formation of voids in the paper structure. On the other hand, the MFC/NFC coating layer has strongly adhered to the paperboard surface (Fig. 6I).

For the *CS 5 %* and *CS 10 %* coatings (Fig. 6 J and 6 M), the surface was more homogeneous than the MFC/NFC. In addition, calcium silicate particles measuring around 2.6 μm, in cube format were observed surrounded by MFC/NFC. The coating layers applied to both *CS 5 %* and *CS 10 %* have strongly adhered to the paperboard, without delamination

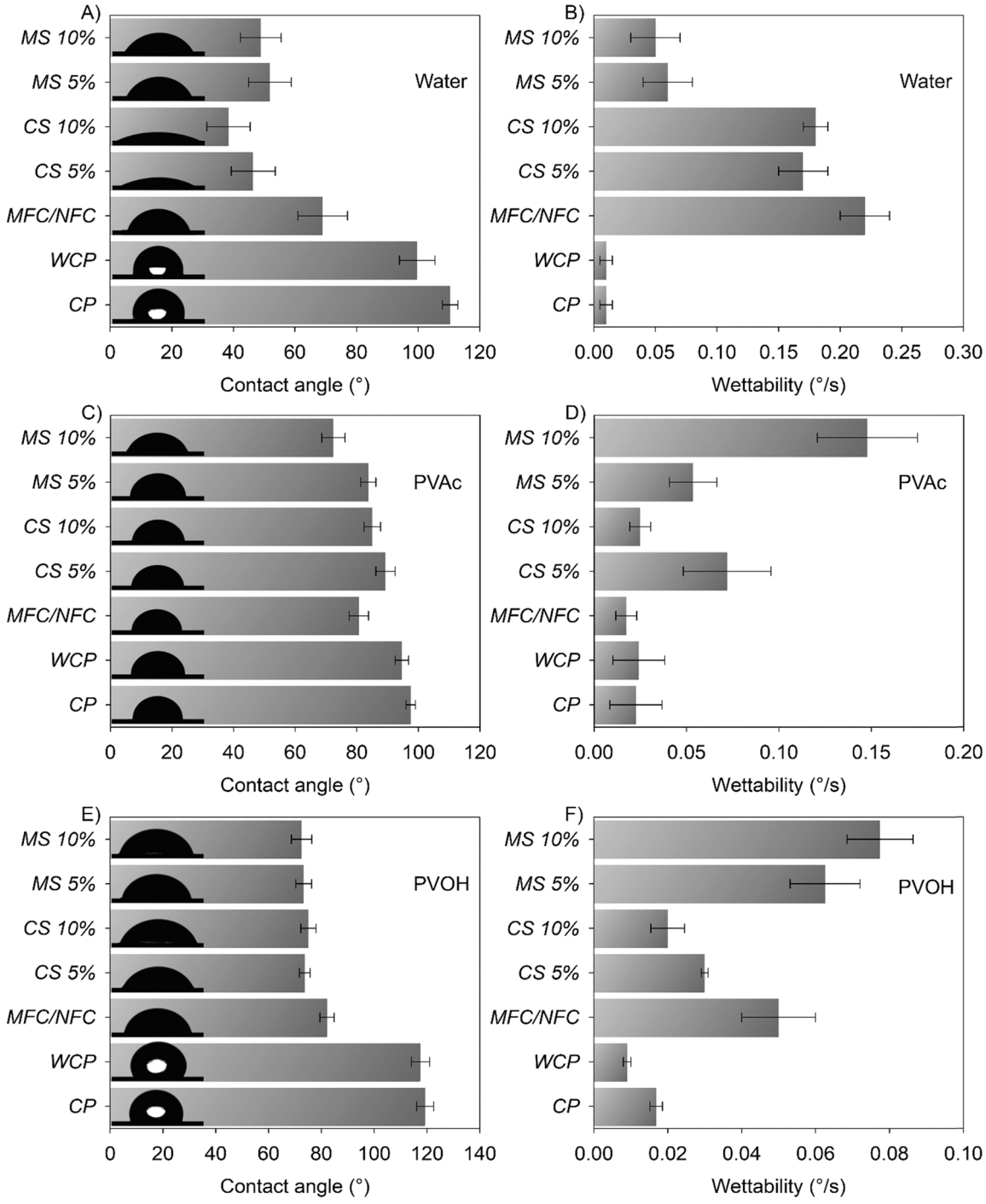

Fig. 7. A) Contact angle with water; B) wettability with water; C) contact angle with PVAc; D) wettability with PVAc; E) contact angle with PVOH; F) PVOH wettability on untreated EUC MFC/NFC coated board and pretreated with calcium silicate and magnesium silicate solutions; The drop images are on the same scale.

(Fig. 6 L and 6 O).

Fig. 5 P and 5 S show that *MS 5 %* and *MS 10 %* coatings reduced irregularities and the number of void spaces on the cardboard surface. Particles of magnesium silicate measuring around 9.2 μm with an aspect of blades were also observed. This corroborates the results obtained in the FTIR, in which the band of 3674 cm^{-1} was verified, attributed to the -OH group of the octahedral sheets of magnesium silicate (Frost and Mendelovici, 2006). Regarding the cross-section, the layer structure of the papers coated with *MS 5 %* and *MS 10 %* was less affected and with smaller gaps concerning the coatings described above (see Figs. 6Q and 6 T). Some gaps were also detected between the most superficial layers of the coating, as can be seen in Fig. 6 R and 6 U. However, these crevices present a lower potential to increase the increase in water absorption than the gaps observed in the layers below the surface, as described for *WCP*, MFC/NFC, and calcium silicate-containing coatings.

The irregularities observed for the papers submitted to wetting and application of coatings can contribute to greater dispersion of water and adhesives on the paper. In general, more irregular surfaces combined with the large amounts of available fillers potentiates the reduction of the contact angle with the surface (Cruz et al., 2022; Mascarenhas et al., 2022a). This effect was observed in the present work. It is possible to verify that the wetting and drying of the paperboard (*WCP*) promoted a reduction of the contact angle with water by around 9.6 % concerning *CP* (~110°) (Fig. 7). However, the wettability was very similar to cardboard in its original condition (~0.01°/s) (Fig. 7B).

The coating composed only of MFC/NFC had a reduced contact angle of about ~37 %, and wettability increased around 20 times about *CP* (0.01°/s), which can be due to the greater contact surface of MFC/NFC and greater exposure of -OH groups (Chen et al., 2022b). The contact angle for *CS 5 %* was around 46° and around 38° for *CS 10 %*. The wettability for these coatings was very close and varied between 0.17° and 0.18°/s. Regarding the *MS 5 %* and *MS 10 %* coatings, the contact angle values were similar and ~45 % lower than CP. The wettability followed the same trend, with values varying around 0.05°/s.

Regarding the test performed with PVAc, *WCP* presented a contact angle very close to those of *CP* (~110°). All the coatings presented a reduction in the contact angle of PVAc with the paper (see Fig. 7C). The highest reduction was observed for *MS 10 %* (~26 %), and the lowest was obtained for *CS 5 %* (~8 %). As for wettability, the highest increases were also observed for *MS 10 %* (~0.14°/s) and *CS 5 %* (~0.07°/s) in relation to *CP* (0.02°/s) (Fig. 7D). For the PVOH test, the contact angle for *CS 5 %*, *CS 10 %*, *MS 5 %*, and *MS 10 %* were around 73 ± 1.1° (see Fig. 7E). For *CP* and *WCP* the values were around ~119° and ~117°, respectively. The contact angles for MFC/NFC were around 10 % higher than those observed for the coated papers. The highest wettability values were obtained for *MS 10 %* (~0.07°/s) and *MS 5 %* (0.06°/s), followed by *MFC/NFC* (0.05°/s), *CS 5 %* (0.03°/s) and *CS 10 %* (0.02°/s) (see Fig. 7F). The wettability values of *CP* and *WCP* were in the same range (~0.01°/s).

The reduction of the contact angles for the conditions evaluated occurred due to the wrinkling of the paper surface. This effect was caused by the swelling and contraction of the fibers due to the adsorption and desorption of water, a consequence of the drying process and application of the coatings (Drelich, 2019). This phenomenon can form pores and expose the macrofibrils, increasing the contact surface with water (Abdelouahab et al., 2021). It can be said that the paper in the original condition had a hydrophobic surface (> 90°), favoring wetting and causing droplet scattering (Zhao and Jiang, 2018). On the other hand, all the coatings applied made the papers more hydrophilic, as the contact angles reduced and the wettability increased, especially for the calcium silicate coatings.

Tsai et al. (2019) observed that the addition of 20–50 % of calcium silicate in composites reinforced with chitosan and titanium alloy promoted the reduction of the contact angle to values below 10°. Kotp et al. (2017) studied the performance of polyamide membranes, concluding that the addition of magnesium silicate nanoparticles reduced the contact angle from ~70° to ~45°, corroborating the results found in this work. These authors explained that calcium and magnesium silicate present a large number of external loads that contribute to greater hydration of the surface and interior of the composite matrices. Another important aspect being considered is that the use of silicates promotes more efficient fibrillation (see Fig. 3). Further, MFC/NFC have a greater surface area and exposure of -OH groups, which contributed to the increase in the number of hydrogen bonds with water, increasing wettability (Lengowski et al., 2020; Xu et al., 2020).

In the context of packaging, reducing the contact angle with PVA can be interesting because it is one of the main adhesives used in the industry. The application of cardboard in multi-layer packaging depends on its ability to spread the adhesive, otherwise, failures in gluing and layer delamination may occur (Antón et al., 2020). In the present work, the coatings showed the potential to improve the distribution of the adhesive and increase the adhesion with other layers (plastics, metals, or other papers). Chen et al. (2022b) observed results similar to this work. These authors verified that the application of MFC/NFC modified with nano-silica for coating paper improved the mechanical strength of multilayer packaging due to the greater interaction of bonds with the other materials that compose the layers. This explanation can be applied to the PVOH, as the applied coatings acted as a kind of primer and favored its spread on the paper surface. Consequently, due to a large number of hydrogen bonds established, the adhesion of PVOH can be potentiated. Thus, the behavior observed for coated papers in this work becomes interesting from an industrial point of view because it can provide better fixation of other coatings without the need for additional surface treatments.

For primary and secondary packaging, used for direct storage with the product and the stock organization (Mahmoudi and Parviziomran, 2020), it can be said that in some applications (drugs, footwear, cereals) high wettability will not always be harmful due to the shorter residence time until reaching the final consumer. These kinds of packaging contain the manufacturer's logo, identification, and information about the composition of the products printed directly on the paper. A higher wettability can contribute to this purpose (Lourenço et al., 2020).

The test of contact angle using printer ink can be interesting in this context. The coating containing only MFC/NFC presented a contact angle 36 % smaller in relation to *CP* (~34.4°), while the values for *WCP* showed differences around ~3 % (Fig. 8A).

The values obtained for *CS 5 %* and *CS 10 %* were ~67 and ~79 % lower concerning *CP*, respectively. On the other hand, *MS 5 %* presented contact angles ~59 % smaller than PC, while for *MS 10 %* the reduction was ~57 %. These results indicate a greater ability to spread and fix the ink on the surface, considering the same volume of ink applied. For *CS 5 %* and *CS 10 %*, the spreading was more uniform (see Figs. 8E and 8F). For *MS 5 %* and *MS 10 %* (see Figs. 8G and 8H), the distribution was more irregular in relation to *CP*, *WCP*, and *MFC/NFC* (see Figs. 8B, 8C, and 8D).

Paper wettability has a high correlation with printability (Aydemir et al., 2020; Ozcan et al., 2021). If the wettability is low, the ink fixation on the paper can be impaired during the handling of boxes and bags, due to friction, ultraviolet radiation (UV), pH variations, and contact with humidity or cleaning products in the gondolas (Ozcan e Kandirmaz, 2020; Zołek-Tryznowska et al., 2020; Genç et al., 2021). Mirmehdi et al. (2018a) observed that the use of MFC/NFC as a coating improved the properties for writing and printing on the paper surface. In addition, coatings act to reduce the surface tension to control and restrict the expansion of ink drops (Mielonen et al., 2015). These characteristics were observed, mainly for coatings containing calcium silicate. The surface free energy also helps to understand these results, as all coated papers showed low surface tension and high surface energy (> 45 mJ/m^2) (see Fig. 8I). The *CS 10 %*, *MS 5 %*, and *MS 10 %* coatings resulted in increases in surface free energy, which were around 4.7 %, 3.2 %, and 6.6 % over *CP* (~45 mJ/m^2), respectively. No considerable increase in surface-free energy was observed when evaluating *WCP*. The

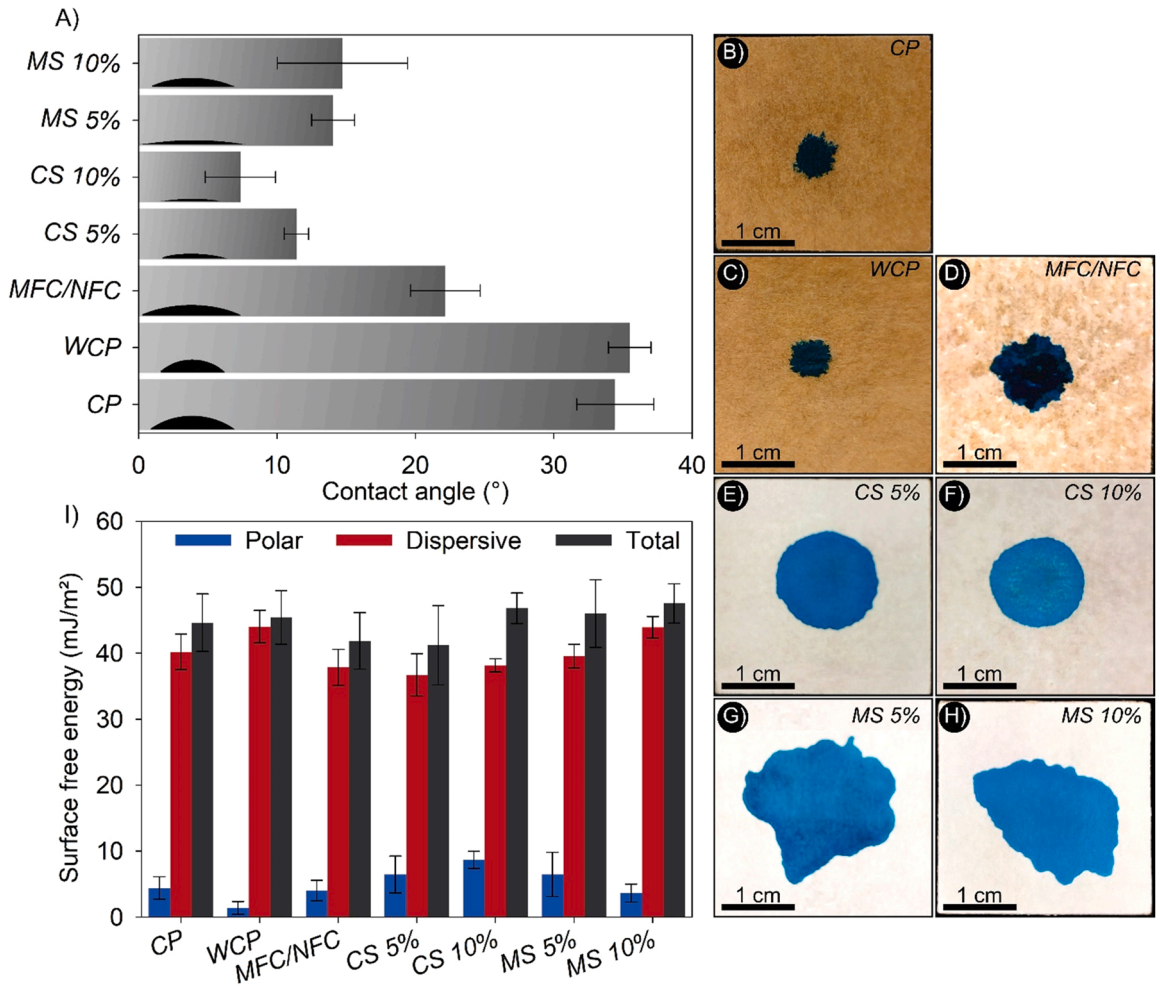

Fig. 8. A) Contact angle, images of the ink spreading on the paper: B) *CP*; C) *WCP*; D) *MFC/NFC*; E) *CS 5 %*; F) *CS 10 %*; G) *MS 5 %*; H) *MS 10 %*, and I) free energy of surface coated with EUC MFC/NFC untreated and pre-treated with calcium and magnesium silicate solutions.

CS 10 % coating increased the polar component energy by approximately 96 % compared to *CP* (~4.4 mJ/m^2). The *CS 5 %* and *MS 5 %* coatings resulted in increases in the polar component of around 47 %, explaining the higher wettability values and the greater spread of ink on the surface of the papers.

Surface free energy allows determining the excess energy on the surface of a solid and can be correlated with the adhesion between different materials as a function of the proportions between polar or dispersive energy (Tanzadeh and Shafabakhsh, 2020; Yongabi et al., 2020). The increase in the surface free energy is related to the presence of hydroxyl groups, responsible for the interaction with polar liquids (Zołek-Tryznowska and Kałuza, 2021). Higher surface energy favors a more efficient distribution of ink and adhesives in coated papers. This aspect is interesting for the industry, as it can contribute to reducing the amount of paint applied and favoring its drying after application (Shenoy and Shetty, 2022). Generally, the industry uses corona treatment to improve the adhesion capacity of the paper (Lopes et al., 2018), the evaluated coatings have the potential to dispense this step, depending on the desired application.

Ozcan et al. (2021) studied the printability with water-based inks and observed that a surface free energy between 40 and 44 mJ/m^2 increased the wettability and printability of the paper. Madeira et al. (2018) reported that surface free energy is also correlated with adhesion strength and can be a tool to assess the quality of multilayer gluing on the packaging.

3.4. Water absorption of the papers

All the coatings provided an increase in Cobb values compared to *CP* (~38 g/m^2) (Fig. 9A). It was also possible to identify a slight increase in water absorption in PCM (~5 %). The Cobb values found for the coating containing only MFC/NFC were ~65 % higher than those observed in PC. This can be explained by the greater exposure of hydroxyl groups, which favored the water absorption and the swelling of the paperboard fibers (Mascarenhas et al., 2022a).

For *CS 5 %*, the Cobb values were increased by ~68 %, while for *CS 10 %*, the increase was around 63 %. Considering the *MS 5 %* and *MS 10 %* coatings, the increments in the Cobb values were around 28.5 % and 49.2 %, respectively. The increases in Cobb can be explained by forming a complex network of microgalleries in the paper layers as a function of the wetting caused by the addition of coatings and by the drying steps (see Fig. 6). The results found are in harmony with other studies. Jeong and Yoo (2020) evaluated cardboard coated with sucrose suspension, beeswax, and whey protein and obtained Cobb values between 60 and 85 g/m^2. Similarly, Shen et al. (2021) obtained Cobb values between 40 and 100 g/m^2 for papers coated with PVA and nanoclay.

Further, as explained above, these coatings increased the wetting and surface energy of the paperboard. However, employing EDS scanning electron microscopy, the presence of Si (blue) and Ca (cyan) was verified, indicating the penetration of silicates in the layers of paperboard at depths ranging from 100 to 150 μm for *CS 5 %* and *CS 10 %* (see Fig. 9B and 9C). Due to the lower viscosity (2600–3300 cP), the *MS 5 %* and *MS*

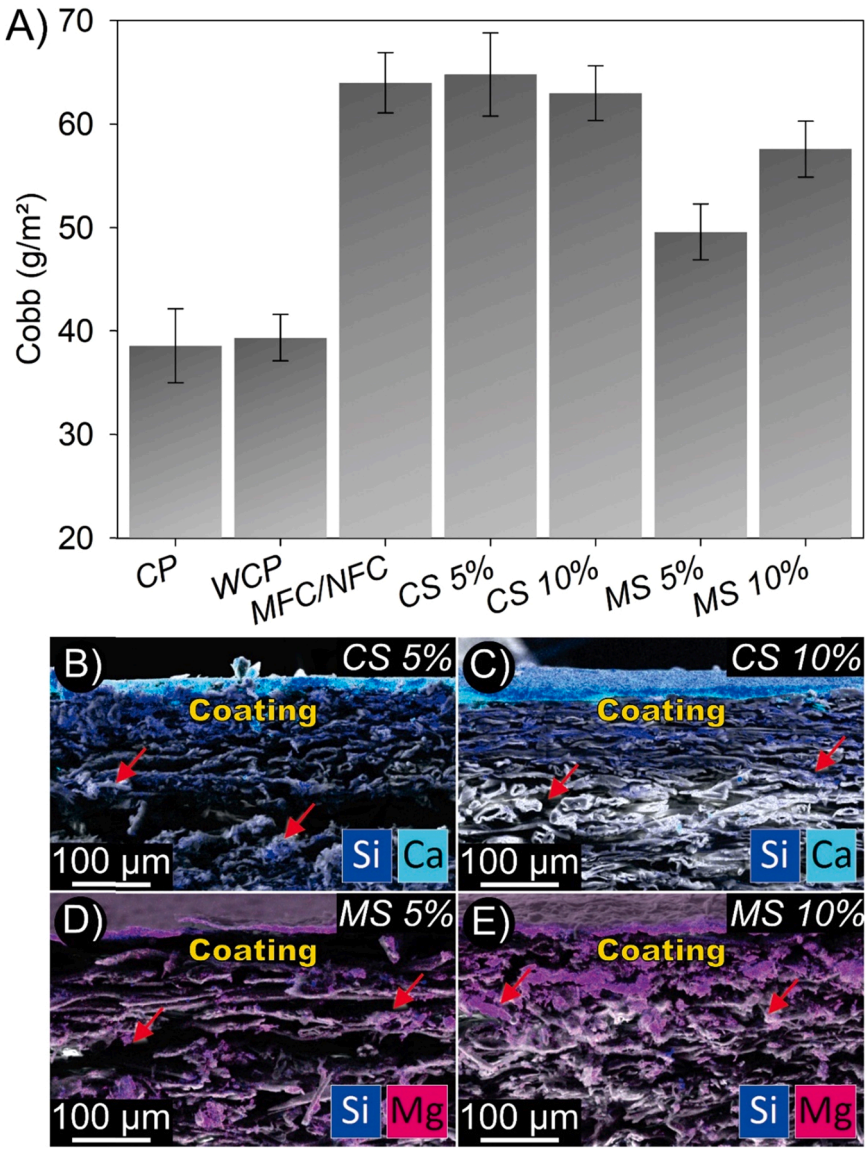

Fig. 9. A) Water absorption (Cobb) and SEM micrographs with EDS of the cardboards cross-sections coated with EUC MFC/NFC untreated and pre-treated with calcium and magnesium silicate solutions; B) *CS 5 %*; C) *CS 10 %*; D) *MS 5 %;* and E) *MS 10 %*.

10 % suspensions penetrated between 250 and 350 µm deep into the paper, as highlighted for Si (blue) and Mg (magenta) in Fig. 9D and Fig. 9E. This potentiated the entry of water into the microgalleries (red arrows in Fig. 9), increasing water absorption in the papers. Adibi et al. (2022) described this behavior when evaluating paper coating with alpha-1–3 glucan and latex. These authors explained that adding the wet layer to the paper surface promotes the swelling of the fibers, which rearrange themselves and form empty spaces between them.

As a result, part of the coating solids was transported along with the solution to the paper's subsurface layers (Fig. 10). After drying, they remain impregnated due to the contraction of the fibers and the establishment of bonds with the cellulose (Thébault et al., 2017). This process can be intensified by adding more layers and performing new drying steps, as observed in the present work.

The amount of research using silicates as a paper coating is minimal, but the application of this material in other conditions can contribute to understanding the results found. Calcium and magnesium silicate are widely used as additives to improve the hydration and cohesion of particles dispersed in cementitious matrices (Cho et al., 2020). These silicates have large amounts of charges available to establish electromagnetic interactions (Sadek et al., 2016; Saedi et al., 2021b), which can be potentiated with MFC/NFC.

Kumar et al. (2011) explained that the retention of calcium-based minerals, sodium silicate, and aluminum silicate on the surface and in the lumen of the fibers could increase the paper's water absorption. By analogy, these hypotheses could be applied to explain the increase in water absorption in paperboard.

It should be noted that the Cobb test is not only used to assess water absorption in the paper. It is also used to determine the ability of glue penetration (Gok and Akpinar, 2020). For papers with low surface energy and Cobb values, some types of adhesive cannot penetrate, leading to the reduced anchorage between the bonded faces. On the other hand, high Cobb values result in excessive adhesive consumption, which can harm bonding and increase production costs. This variable is crucial in the production of multilayer packaging, as the paper must promote adequate adhesion to the other layers (metals or plastics) to guarantee the barrier to gases and mechanical resistance. Dohr and Hirn (2020) found that adhesive penetration is strongly related to the strength of Kraft sack paper. The authors explained that surface sizing could result in delamination problems between the layers due to the smaller chemical and physical anchorages in the voids located in the subsurface layers of the paper.

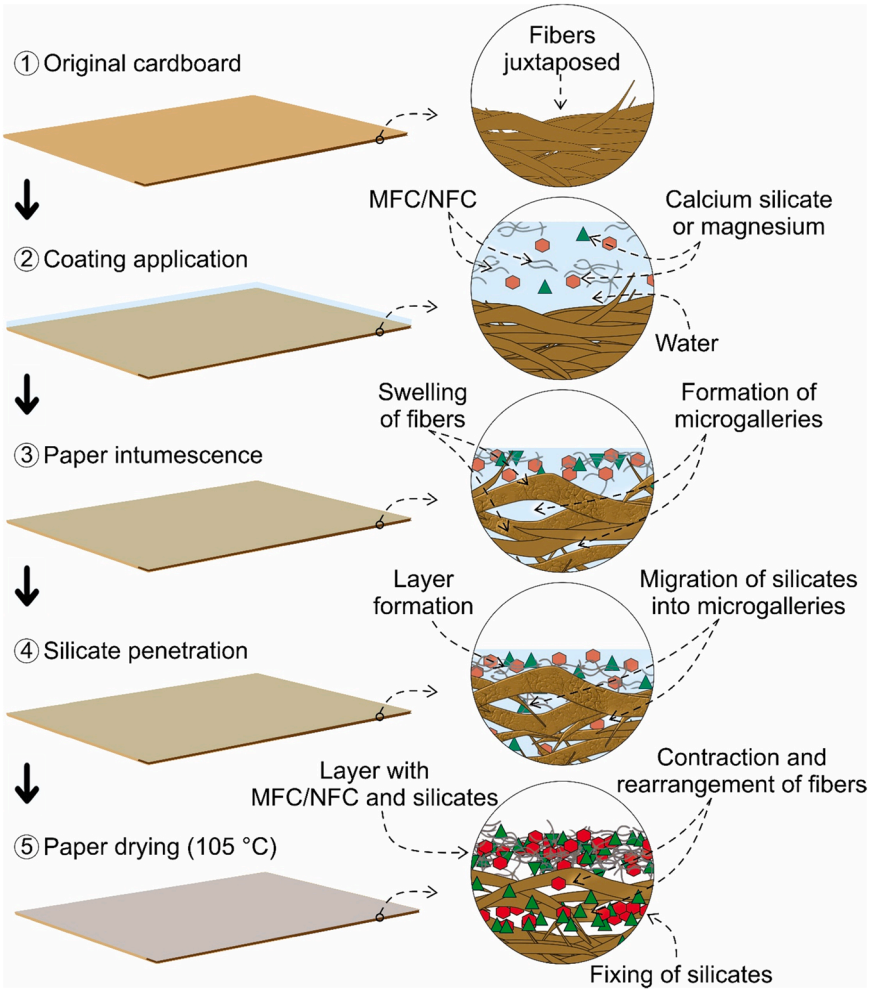

Fig. 10. Steps and mechanisms of penetration of the silicates suspensions in the cardboard.

3.5. *Water vapor permeability and mechanical properties of the papers*

For *WCP*, the wetting and drying stages contributed to a slight increase in the values of WVTR and WVP in the order of 2.5 % and 5 %, respectively, concerning *CP* (Figs. 11A and 11B). This was assumed to be due to the increase in the number of empty spaces and microgalleries between the layers of the paperboard, facilitating the passage of water vapor.

The coating of cardboard with MFC/NFC resulted in a reduction of WVTR by ~6 %, and for the WVP, it was very similar to that observed for *CP* (~105 g mm/kPa^{-1} day m^2). The reduction in WVTR is related to the characteristics of the MFC/NFC film on the paper surface, which has a structure with organized layers, very tangled, and higher density, making it difficult for the passage of gases (Wang et al., 2020; Hashemzehi et al., 2022).

About *CS 5 %*, the WVTR was very close to the observed for *CP* (~1265 g/m^2 day), while for *CS 10 %*, a reduction of ~4.2 % was observed. For WVP, a slight increase (~4.7 %) of the values for the *CS 5 %* coating was observed. The best barrier properties were obtained using the *MS 5 %* and *MS 10 %* coatings, for which WVTR obtained reductions of ~12 % and ~5.5 % in relation to *CP*, respectively. As for WVP, *MS 5 %* promoted a reduction of ~14 %, while for *MS 10 %*, no substantial differences were observed with the other coatings.

Despite the formation of microgalleries, the reductions observed for the calcium and magnesium silicate coatings are due to the impregnation of subsurface layers of the cardboard, as shown in Figs. 9 and 10. The silicate particles occupied a large part of the void spaces between the fibers, and in the MFC/NFC network, reducing the flow of water vapor through the layers of the paper. Similarly, Kumar et al. (2011) explained that adding minerals (aluminum silicate and limestone fillers) promotes the occupation of pits, lumen, and mesopores with dimensions of 2–100 nm in diameter present in the fibers and between the fibers. This effect was most prominent for magnesium silicate due to the blade shape of the particles (see Fig. 6).

Huang et al. (2018) explained that this feature contributes to better dispersing particles in paper microgalleries. Rastogi and Samyn (2015) demonstrated that the barrier properties of a coating composed of silicates depend on its state of aggregation, dispersion, and orientation of the layers. In general, the results are in harmony with other works in the literature. Chen et al. (2022b) obtained WVTR between 1200 and 2000 g/m^2 day for MFC and nano-silica coated papers.

Wang et al. (2022) obtained WVTR ranging between 1200 and 1500 g/m^2 day for paperboard, with a basis weight of 300 g/m^2, coated with carboxymethyl cellulose sodium and carboxymethyl chitosan. Marzbani et al. (2021), on the other hand, obtained WVP values ranging from 108 to 573 g mm/kPa^{-1} day m^2 when evaluating paperboard coating with different concentrations between polyethylene wax and soy protein-based. Considering possible applications for coated papers, Wang et al. (2018) showed that WVTR values between 1000 and 10, 000 g/m^2 day indicate that the film/paper can be applied in packaging bakery products and cheeses, fruits, and vegetables.

The values of tensile strength and Young's modulus for *WCP* were ~53 and ~59 % for CP, respectively, which indicates that wetting and drying contributed to the reduction of the mechanical strength of the

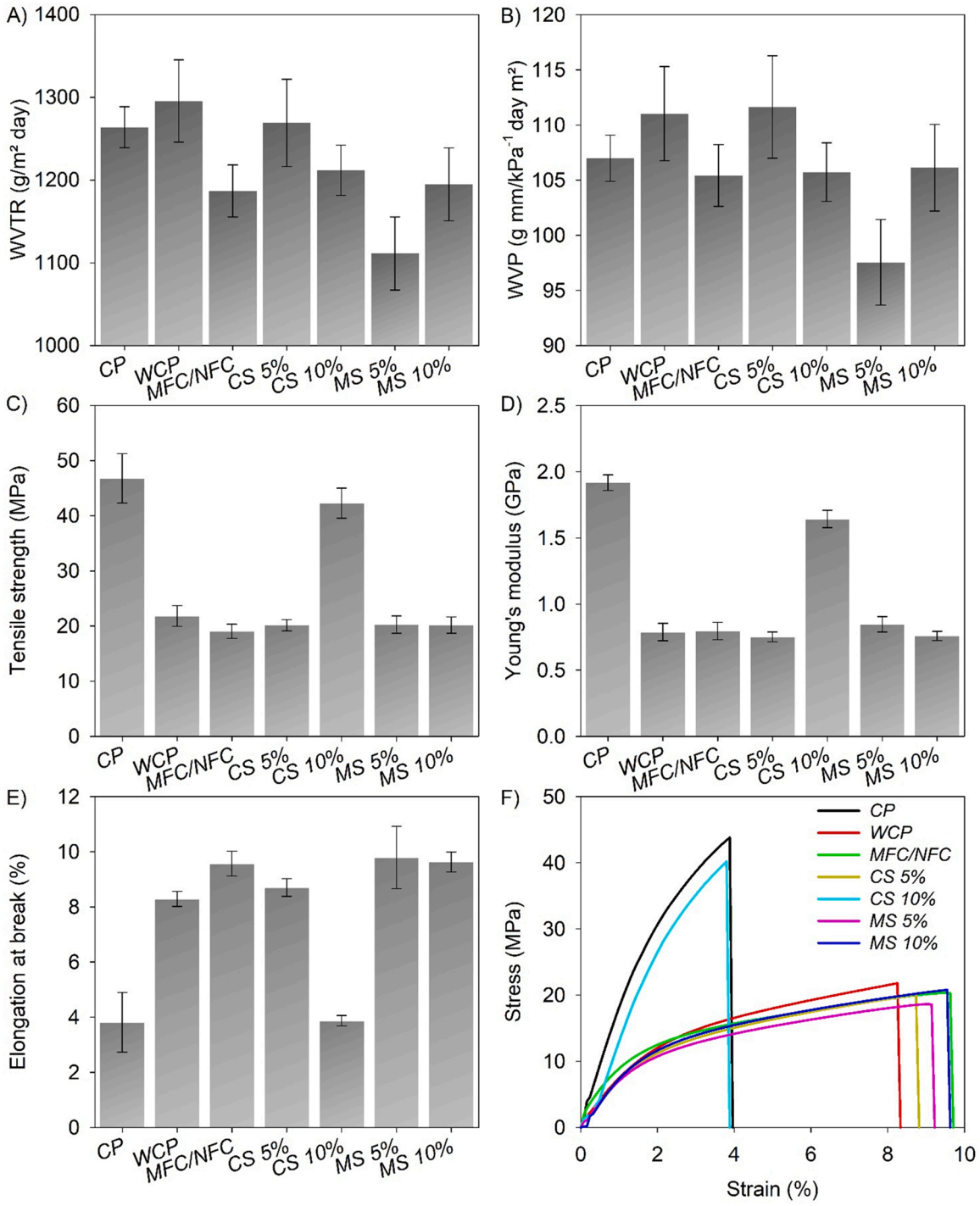

Fig. 11. A) WVTR; B) WVP; C) tensile strength; D) Young's modulus; E) elongation at break; and F) stress x strain curves in the tensile test of cardboard coated with EUC MFC/NFC untreated and pre-treated with calcium and magnesium silicate solution.

papers (Fig. 11C and D). The tensile strength and Young modulus for MFC/NFC, *CS 5 %*, *MS 5 %*, and *MS 10 %* were very similar and were in the range of 20.2 ± 0.06 MPa and 0.79 ± 0.05 GPa, respectively. For *CS 10 %*, the results for tensile strength (~42 MPa) and Young's modulus (~1.6 GPa) were slightly lower than those observed for CP. Cataldi et al. (2019) and Wohlert et al. (2022) explained that over time water can plasticize (soften) and hydrolyze cellulose and its derivatives. These two phenomena alter and destabilize the cellulosic structures in the paper. Roig et al. (2011) found that this effect is due to the physical aging of the paper and the relaxation of cellulose β 1–4 bonds.

Salmén and Larsson (2018) exposed that temperature and humidity induce the softening of lignocellulosic fibers. The action of water in this context is known as "hygroplastification", which consists of reducing the glass transition temperature and the stiffness of the cell wall after being subjected to different steps of water sorption. Haslach Junior (2000) pointed out that paper mechanical properties significantly depend on the responses to applied loads, humidity, and temperature. The authors explained that successive wetting and drying processes cause the fibers to move apart and reduce the interactions between the cellulose molecules, as the hydrogen bonds become very weak. This is due to the effect of hysteresis that prevents the fibers from returning to their original condition after drying-induced contraction (Salmén and Larsson, 2018).

These explanations clarify the results, as the wetting and drying process during the coatings possibly promoted accelerated aging, intensifying the action of water in breaking hydrogen bonds and reducing the adhesion between the fibers. For the case of *CS 10 %*, the low reduction in mechanical strength can be explained by the higher viscosity (~4900 cP), lower water penetration, and stronger anchorage of the coating on the paper surface, as seen in Fig. 8C. In higher concentrations, MFC/NFC and calcium silicate formed larger tangles (see Fig. 6 M). This increased the amount of substances with higher hygroscopic potential, favoring the retention of water on the surface, preventing the swelling of the deeper layers, and preserving the structure of the paper.

Tensile strength indicates the strength of paper and paperboard, which depends on factors such as sizing, fiber length, and fiber strength (Aboura et al., 2004). Assessing the deformation, ductility, and tensile energy absorption in the tensile test can help predict the cardboard performance, particularly when the material is subjected to unequal stresses (Fadiji et al., 2018). The coatings made the paper more malleable due to the greater deformation capacity (see Figs. 11E and 11F). Except for PC (3.8 %) and *CS 10 %* (3.9 %), the other coatings showed elongation at break ranging between 8.5 % and 9.8 %.

Mirmehdi et al. (2018b) also found that increasing nanoclay contents in MFC/NFC suspensions in paper coating resulted in a reduction of mechanical strength in the order of 33 % compared to those without nanoclays. Similar results were obtained by Oliveira et al. (2022), which attributed this effect to the hornification of the fibers due to the wetting and drying cycles of the paper during the application of the coatings with NFC and silica. Franke et al. (2020) evaluated paperboard coated with plastic multilayers and obtained improvements in paperboard formability, as observed in the present work. The authors found that the coated papers showed a reduction in tensile strength from 70 MPa to 30 MPa and Young's modulus was reduced from 6.5 GPa to 2.5 GPa.

The ductility is an interesting feature in the packaging (Marsh and Bugusu, 2007), as it allows the paper to be folded for the production of boxes of different formats or transport in the form of reels without breaking the fibers. Fadiji et al. (2018) pointed out that when low ductility is detected in a tensile test, the low fracture strength of paperboard under other loading forms is often observed. Vishtal and Retulainen (2012) exposed that ductility is related to formability, which is the ability of the material to undergo plastic deformation without damage. These authors explain that this feature is crucial for cardboard-based materials, as it enables the production of paper trays, cups, paper plates, paper tubes, food containers, and various consumer packaging using the *deep-drawing* method.

Considering the characteristics presented, the coated papers have more interesting properties for application in multilayer packaging than uncoated paper. In addition to mechanical properties, papers coated with calcium and magnesium silicates improved the ability to spread and absorb adhesives, other coating layers, and ink on the paperboard, which can increase the adhesion capacity with other materials or printability. Furthermore, it was observed that there was an improvement in the performance of the paper's ability to prevent the passage of water vapor.

4. Conclusion

The pre-treatments with calcium silicate reduced water retention in the fibers. The FTIR observed new functional groups in cellulose (O-Si-O, Mg-OH, Si-O-Ca, Si-O-Si). Pre-treatments reduced energy consumption in the production of micro/nanofibrils (~30 %). Coatings with the suspensions reduced the amount of void space on the surface of the paperboard. In the cross-section, microgalleries were formed due to the paper wetting and drying cycles, especially for MFC/NFC, *CS 5 %*, and *CS 10 %*. The formation of layers with micro/nanofibrils without and with silicates on the surface and subsurface of the paperboard improved the barrier properties, making them suitable for application in bread, cheese, fruits, and vegetable packaging. MFC/NFC, *CS 5 %*, and *CS 10 %* increased the water spread on the paperboard's surface. The highest wettabilities were observed for *CS 5 %* and *MS 10 %* in the assay conducted with PVAc. For PVOH, the highest wettability was obtained for MFC/NFC, *MS 5 %*, and *MS 10 %*, suggesting improvements in adhesive anchoring and adhesion with other coating layers. The coatings increased the spread of ink on the surface of the paper. The strength and stiffness of the papers were reduced due to wetting and drying during the application of the coatings. There was an increase in elasticity, which enhances the formability of paperboard for applications in packaging with different formats. Optimizing application and drying techniques for MFC/NFC and silicate coating formulations can improve the coated packaging papers' mechanical and barrier properties.

CRediT authorship contribution statement

Adriano Reis Prazeres Mascarenhas: Investigation, Visualization, Data presentation, Writing – original draft. **Mário Vanoli Scatolino**: Visualization, Data presentation, Investigation, Writing – original draft. **Matheus Cordazzo Dias:** Visualization, Data presentation, Investigation, Writing – original draft. **Mendonca Maressa Carvalho Mendonça:** Visualization, Data presentation, Investigation, Writing – original draft. **Rafael Rodolfo de Meloe:** Conceptualization, Visualization, Data presentation, Writing – review & editing. **Maria Alice Martins**: Resources, Project administration, Funding acquisition, Supervision. **Gustavo Henrique Denzin Tonoli:** Resources, Project administration, Funding acquisition, Supervision.

Declaration of Competing Interest

The authors declare that they have no known competing financial interests or personal relationships that could have appeared to influence the work reported in this paper.

Data Availability

Data will be made available on request.

Acknowledgment

We are especially grateful to the Graduate Program in Wood Science and Technology (PPGCTM) of the Federal University of Lavras (UFLA) for providing study material and infrastructure. We thank the Electronic Microscopy Laboratory (LME) of UFLA for obtaining scanning images. The authors are also grateful to the Coordination for the Improvement of Higher Education Personnel (CAPES) for providing research grants. The research was funded by the National Council for Scientific and Technological Development (CNPq finance code 314203/2018-4) and Fundação de Amparo à Pesquisa do Estado de Minas Gerais (FAPEMIG finance code CAG APQ-03248-17). We also thank the and Fundação de Amparo à Pesquisa do Estado do Amapá (FAPEAP), and the State University of Amapá for the postdoctoral scholarships (financial code: 0022.0279.1202.0016/2021 - PROPESP).

References

Abdelouahab, N.B., Gossard, A., Ma, X., Dialla, H., Maillet, B., Rodts, S., Coussot, P., 2021. Understanding mechanisms of drying of a cellulose slurry by magnetic resonance imaging. Cellulose 28, 5321–5334. https://doi.org/10.1007/s10570-021-03916-5.

Aboura, Z., Talbi, N., Allaoui, S., Benzeggagh, M.L., 2004. Elastic behavior of corrugated cardboard: experiments and modeling. Compos. Struct. 63, 53–62. https://doi.org/10.1016/S0263-8223(03)00131-4.

Adibi, A., Valdesueiro, D., Mok, J., Behabtu, N., Lenges, C., Simon, L., Mekonnen, T.H., 2022. Sustainable barrier paper coating based on alpha-1,3 glucan and natural rubber latex. Carbohydr. Polym. 282, 119121 https://doi.org/10.1016/j.carbpol.2022.119121.

Al-Oweini, R., El-Rassy, H., 2009. Synthesis and characterization by FTIR spectroscopy of silica aerogels prepared using several $Si(OR)_4$ and R" $Si(OR')_3$ precursors. J. Mol. Struct. 919, 140–145. https://doi.org/10.1016/j.molstruc.2008.08.025.

Ang, S., Haritos, V., Batchelor, W., 2019. Effect of refining and homogenization on nanocellulose fiber development. Sheet Strength, Energy Consum. Cellul. 26, 4767–4786. https://doi.org/10.1007/s10570-019-02400-5.

Antón, N., González-Fernandez, A., Villarino, 2020. Reliability and mechanical properties of materials recycled from multilayer flexible packages. Materials 13, 3992. https://doi.org/10.3390/ma13183992.

Arantes, A.C.C., Silva, L.E., Wood, D.F., Almeida, C.G., Tonoli, G.H.D., Oliveira, J.E., Silva, J.P., Williams, T.G., Orts, W.J., Bianchi, M.L., 2019. Bio-based thin films of cellulose nanofibrils and magnetite for potential application in green electronics. Carbohydr. Polym. 207, 100–107. https://doi.org/10.1016/j.carbpol.2018.11.081.

ASTM Standard, 2005. ASTM D3285–93, Standard Test Method for Water Absorptiveness of Nonbibulous Paper and Paperboard (Cobb Test).

ASTM Standard, 2012. E-104–02, Standard Practice for Maintaining Constant Relative Humidity by Means of Aqueous Solutions.

ASTM Standard, 2016a. ASTM E-96, Standard Test Methods for Water Vapor Transmission of Materials.

ASTM Standard, 2016b. ASTM D828–16e1, Standard Test Method for Tensile Properties of Paper and Paperboard Using Constant-Rate-of-Elongation Apparatus.

ASTM Standard, 2022. ASTM D7490–13, Standard Test Method for Measurement of the Surface Tension of Solid Coatings, Substrates, and Pigments using Contact Angle Measurements.

Aydemir, C., Altay, B.N., Akyol, M., 2020. Surface analysis of polymer films for wettability and ink adhesion. Color Res. Appl. 46, 489–499. https://doi.org/10.1002/col.22579.

Bhattacharjee, S., 2016. DLS and zeta potential – what they are and what they are not. J. Control. Release 235, 337–351. https://doi.org/10.1016/j.jconrel.2016.06.017.

Blanco, A., Monte, M.C., Campano, C., Balea, A., Merayo, N., Negro, C., 2018. Nanocellulose for industrial use: cellulose nanofibers (CNF), cellulose nanocrystals (CNC), and bacterial cellulose (BC). In: Hussain, C.M. (Ed.), Handbook of Nanomaterials for Industrial Applications. Elsevier, Amsterdam, pp. 74–126.

Cataldi, P., Profaizer, M., Bayer, I.S., 2019. Preventing water-induced mechanical deterioration of cardboard by a sequential polymer treatment. Ind. Eng. Chem. Res. 58, 6456–6465. https://doi.org/10.1021/acs.iecr.9b00712.

Chen, H., Wang, B., Li, J., Ying, G., Chen, K., 2022b. High-strength and super-hydrophobic multilayered paper based on nano-silica coating and micro-fibrillated cellulose. Carbohydr. Polym. 288, 119371 https://doi.org/10.1016/j.carbpol.2022.119371.

Chen, M., Li, L., Zhao, P., Wang, S., Lu, L., 2019. Paper sludge functionalization for achieving fiber-reinforced and low thermal conductivity calcium silicate insulating materials. J. Therm. Anal. Calorim. 136, 493–503. https://doi.org/10.1007/s10973-018-7682-0.

Chen, S., Yue, N., Cui, M., Penkova, A., Huang, R., Qi, W., He, Z., Su, R., 2022a. Integrating direct reuse and extraction recovery of TEMPO for production of cellulose nanofibrils. Carbohydr. Polym. 294, 119803 https://doi.org/10.1016/j.carbpol.2022.119803.

Cho, B.H., Chung, W., Nam, B.H., 2020. Molecular dynamics simulation of calcium-silicate-hydrate for nano-engineered cement composites - a review. Nanomaterials 10, 2158. https://doi.org/10.3390/nano10112158.

Cruz, T.M., Mascarenhas, A.R.P., Scatolino, M.V., Faria, D.L., Matos, L.C., Duarte, P.J., Moreira Neto, J., Mendes, L.M., Tonoli, G.H.D., 2022. Hybrid films from plant and bacterial nanocellulose: mechanical and barrier properties. Nord. Pulp Pap. Res. J. 37, 159–174. ⟨https://orcid.org/0000-0001-6623-5310⟩.

Darghouth, A., Aouida, S., Bessais, B., 2021. High purity porous silicon powder synthesis by magnesiothermic reduction of Tunisian silica sand. Silicon 13, 667–676. https://doi.org/10.1007/s12633-020-00433-1.

Dey, A., Dhumal, C.V., Sengupta, P., Kumar, A., Pramanik, N.K., Alam, T., 2021. Challenges and possible solutions to mitigate the problems of single-use plastics used for packaging food items: a review. J. Food Sci. Technol. 58, 3251–3269. https://doi.org/10.1007/s13197-020-04885-6.

Dias, M.C., Mendonça, M.C., Damásio, R.A.P., Zidanes, U.L., Mori, F.A., Ferreira, S.R., Tonoli, G.H.D., 2019. Influence of hemicellulose content of *Eucalyptus* and *Pinus* fibers on the grinding process for obtaining cellulose micro/nanofibrils. Holzforschung 73, 1035–1046, 2019.

Dimic-Misic, K., Puisto, A., Gane, P., Nieminen, K., Alava, M., Paltakari, J., Maloney, T., 2013. The role of MFC/NFC swelling in the rheological behavior and dewatering of high consistency furnishes. Cellulose 20, 2847–2861. https://doi.org/10.1007/s10570-013-0076-3.

Dohr, C.A., Hirn, U., 2020. Influence of paper properties on adhesive strength of starch gluing. Nord. Pulp Pap. Res. J. 37, 120–129. https://doi.org/10.1515/npprj-2021-0039.

Drelich, J.W., 2019. Contact angles: From mistakes to new developments through liquid-solid adhesion measurements. Adv. Colloid Interface Sci. 267, 1–14. https://doi.org/10.1016/j.cis.2019.02.002.

Fadiji, T., Berry, T.M., Coetzee, C.J., Opara, U.L., 2018. Mechanical design and performance testing of corrugated paperboard packaging for the postharvest handling of horticultural produce. Biosyst. Eng. 171, 220–224. https://doi.org/10.1016/j.biosystemseng.2018.05.004.

Foster, E.J., Moon, R.J., Agarwal, U.P., Bortner, M.J., Bras, J., Espinosa, S.C., Chan, K.J., Clift, M.J.D., Cranston, E.D., Eichhorn, S.J., Fox, D.M., Hamad, W.Y., Heux, L., Jean, B., Korey, M., Nieh, W., Ong, K.J., Reid, M.S., Renneckar, S., Roberts, R., Shatkin, J.A., Simonsen, J., Bagby, K.S., Wanasekara, N., Youngblood, J., 2018. Current characterization methods for cellulose nanomaterials. Chem. Soc. Rev. 47, 2511–3006. https://doi.org/10.1039/C6CS00895J.

Franke, W., Leminen, V., Groche, P., Varis, J., 2020. The effects of pretreatment and coating on the formability of extrusion-coated multilayer paperboard–plastic composites. Packag. Technol. Sci. 34, 105–116. https://doi.org/10.1002/pts.2542.

French, A.D., 2014. Idealized powder diffraction patterns for cellulose polymorphs. Cellulose 21, 885–896. https://doi.org/10.1007/s10570-013-0030-4.

Frost, R.L., Mendelovici, E., 2006. Modification of fibrous silicate surfaces with organic derivatives: An infrared spectroscopic study. J. Colloid Interface Sci. 294, 47–52. https://doi.org/10.1016/j.jcis.2005.07.014.

Genç, H.Y.G., Sönmez, S., Öznur, Ö., Akgül, A., Çetiner, B.N., 2021. Printability of bio-composite sheets made from paper mill and cardboard mill waste sludge. print 1–9. https://doi.org/10.1108/PRT-06-2021-0060.

Gok, B., Akpinar, D., 2020. Investigation of strength and migration of corrugated cardboard boxes. Hittite J. Sci. Eng. 7, 163–168. https://doi.org/10.17350/HJSE19030000185.

Gorur, Y.C., Larsson, P.A., Wagberg, L., 2020. Self-fibrillating cellulose fibers: rapid in situ nanofibrillation to prepare strong, transparent, and gas barrier nanopapers. Biomacromolecules 21, 1480–1488. https://doi.org/10.1021/acs.biomac.0c00040?ref=pdf.

Guimarães Júnior, M., Teixeira, F.G., Tonoli, G.H.D., 2015. Preparation of cellulose nanofibrils from bamboo pulp by mechanical defibrillation for their applications in biodegradable composites. J. Nanosci. Nanotechnol. 15, 1–18. https://doi.org/10.1166/jnn.2015.10854.

Gupta, P., Verma, C., Maji, P.K., 2019. Flame retardant and thermally insulating clay-based aerogel facilitated by cellulose nanofibers. J. Supercrit. Fluids 152, 104537. https://doi.org/10.1016/j.supflu.2019.05.005.

Hashemzehi, M., Mesic, B., Sjöstrand, B., Naqvi, M., 2022. A comprehensive review of nanocellulose modification and applications in papermaking and packaging: challenges, technical solutions, and perspectives. BioResources 17, 1–63.

Haslach Junior, HW, 2000. The moisture and rate-dependent mechanical properties of paper: a review. Mech. Time-Depend. Mater. 4, 169–210. https://doi.org/10.1023/A:1009833415827.

Hofmeister, A.M., Bowey, J.E., 2006. Quantitative infrared spectra of hydrosilicates and related minerals. Mon. Not. R. Astron. Soc. 367, 577–591. https://doi.org/10.1111/j.1365-2966.2006.09894.x.

Huang, R., He, Li, Zhang, T., Li, D., Tang, P., Feng, Y., 2018. Novel carbon paper@ magnesium silicate composite porous films: design, fabrication, and adsorption behavior for heavy metal ions in aqueous solution. ACS Appl. Mater. Interfaces 10, 22776–22785. https://doi.org/10.1021/acsami.8b01557.

Hubbe, M.A., Venditti, R.A., Rojas, O.J., 2007. What happens to cellulosic fibers during papermaking and recycling? a review. BioResources 2, 739–788.

Ikramullah, S.R., Thalib, S., Huzni, S., 2014. Hemicellulose and lignin removal on typha fiber by alkali treatment, 352. IOP Publishing,. https://doi.org/10.1088/1757-899X/352/1/012019.

Jeevanandam, J., Chan, Y.S., Danquah, M.K., 2017. Biosynthesis and characterization of MgO nanoparticles from plant extracts via induced molecular nucleation. N. J. Chem. 00, 1–3. https://doi.org/10.1039/x0xx00000x.

Jeong, S., Yoo, S.R., 2020. Whey protein concentrate-beeswax-sucrose suspension-coated paperboard with enhanced water vapor and oil-barrier efficiency. Food Packag. Shlef Life 25, 100530. https://doi.org/10.1016/j.fpsl.2020.100530.

Jia, N., Li, S.M., Ma, M.G., Zhu, J.F., Sun, R.C., 2011. Syntesis and characterization of cellulose-silica composite fiber in ethanol/water mixed solvents. Bioresources 6, 1186–1195.

Jin, F., Al-Tabbaa, A., 2013. Thermogravimetric study on the hydration of reactive magnesia and silica mixture at room temperature. Thermochim. Acta 566, 162–168. https://doi.org/10.1016/j.tca.2013.05.036.

Jin, K., Tang, Y., Liu, J., Wang, J., Ye, C., 2021. Nanofibrillated cellulose as coating agent for food packaging paper. Int. J. Biol. Macromol. 168, 331–338. https://doi.org/10.1016/j.ijbiomac.2020.12.066.

Khadraoui, M., Khiari, R., Bergaoui, L., Mauret, E., 2022. Production of lignin-containing cellulose nanofibrils by the combination of different mechanical processes. Ind. Crops Prod. 183, 114991 https://doi.org/10.1016/j.indcrop.2022.114991.

Khan, A., Rehmat, U., Shah, L.A., Usman, M., 2020. Effect of experimental variables on the physicochemical characteristics of multi-responsive cellulose-based polymer microgels. Colloid Chem. Electrochem. 94, 1503–1541. https://doi.org/10.1134/S003602442007016X.

Kotp, Y.H., Shelb, Y.A., El-Deab, M.S., El-Anadouli, B.E., Sawky, H.A., 2017. Performance enhancement of PA-TFC RO membrane by using magnesium silicate nanoparticles. J. Inorg. Organomet. Polym. Mater. 27, 201–214. https://doi.org/10.1007/s10904-017-0667-9.

Kumar, P., Negi, Y.S., Singh, S.P., 2011. Filler loading in the lumen or/and cell wall of fibers – a literature review. BioResources 6, 3526–3546.

Lengowski, E.C., Bonfatti Júnior, E.A., Simon, L., Muñiz, G.I.B., Andrade, A.S., Nisgoski, S., Klock, U., 2020. Different degree of fibrillation: strategy to reduce permeability in nanocellulose-starch films. Cellulose 27, 10855–10872. https://doi.org/10.1007/s10570-020-03232-4.

Li, L., Zhang, M., Song, S., Yang, B., Wu, Y., Yang, Q., 2018. Preparation of core/shell structured silicate composite filler and its reinforcing property. Powder Technol. 332, 27–32. https://doi.org/10.1016/j.powtec.2018.03.037.

Li, M.C., Wu, Q., Moon, R.J., Hubbe, M.A., Bortner, M.J., 2021. Rheological aspects of cellulose nanomaterials: governing factors and emerging applications. Adv. Mater. 33, 2006052 https://doi.org/10.1002/adma.202006052.

Li, S.M., Jia, N., Zhu, J.F., Ma, M.G., Sun, R.C., 2010. Synthesis of cellulose-calcium silicate nanocomposites in ethanol/water mixed solvents and their characterization. Carbohydr. Polym. 80, 270–275. https://doi.org/10.1016/j.carbpol.2009.11.024.

Liu, C., Du, H., Dong, L., Wang, X., Zhang, Y., Yu, G., Li, B., Mu, X., Peng, H., Liu, H., 2017. Properties of nanocelluloses and their application as rheology modifier in

paper coating. Ind. Eng. Chem. Res. 56, 8264–8273. https://doi.org/10.1021/acs.iecr.7b01804.
Liu, C., Zhang, W., Song, S., Li, H., 2019. A novel method to improve carboxymethyl cellulose performance in the flotation of talc. Miner. Eng. 131, 23–27. https://doi.org/10.1016/j.mineng.2018.11.003.
Lopes, T.A., Bufalino, L., Claro, P.I.C., Martins, M.A., Tonoli, G.H.D., Mendes, L.M., 2018. The effect of surface modifications with corona discharge in *Pinus* and *Eucalyptus* nanofibril films. Cellulose 25, 5017–5033. https://doi.org/10.1007/s10570-018-1948-3.
Lourenço, A.F., Gamelas, J.A.F., Sarmento, P., Ferreira, P.J.T., 2020. Cellulose micro and nanofibrils as coating agents for improved printability in office papers. Cellulose 27, 6001–6010. https://doi.org/10.1007/s10570-020-03184-9.
Lu, P., Zhao, H., Zheng, L., Duan, Y., Wu, M., Yu, X., Yang, Y., 2022. Nanocellulose/Nisin hydrogel microparticles as sustained antimicrobial coatings for paper packaging. ACS Appl. Polym. Mater. 4, 2664–2673. https://doi.org/10.1021/acsapm.2c00001.
Madeira, D.M.F., Vieira, O., Pinheiro, L.A., Carvalho, B.M., 2018. Correlation between surface energy and adhesion force of polyethylene/paperboard: a predictive tool for quality control in laminated packaging. Int. J. Chem. Eng. 2018, 2709037 https://doi.org/10.1155/2018/2709037.
Mahmoudi, M., Parviziomran, I., 2020. Reusable packaging in supply chains: a review of environmental and economic impacts, logistics system designs, and operations management. Int. J. Prod. Econ. 228, 107730 https://doi.org/10.1016/j.ijpe.2020.107730.
Marsh, K., Bugusu, B., 2007. Food packaging—roles, materials, and environmental issues. J. Food Sci. 72, 39–55. https://doi.org/10.1111/j.1750-3841.2007.00301.x.
Martins, C.C.N., Dias, M.C., Mendonça, M.C., Durães, A.F.S., Silva, L.E., Félix, J.R., Damásio, R.A.P., Tonoli, G.H.D., 2021. Optimizing cellulose microfibrillation with NaOH pretreatments for unbleached Eucalyptus pulp. Cellulose 28, 11519–11531. https://doi.org/10.1007/s10570-021-04221-x.
Marzbani, P., Azadfallah, M., Yousefzadeh, M., Najafi, F., Pourbabaee, A.A., Koivula, H., Ritala, M., 2021. Effect of polyethylene wax/soy protein-based dispersion barrier coating on the physical, mechanical, and barrier characteristics of paperboards. J. Coat. Technol. Res. 18, 247–257. https://doi.org/10.1007/s11998-020-00403-7.
Mascarenhas, A.R.P., Scatolino, M.V., Santos, A.A., Norcino, L.B., Duarte, P.J., Melo, R. R., Dias, M.C., Faria, C.E.T., Mendonça, M.C., Tonoli, G.H.D., 2022a. Hydroxypropyl methylcellulose films reinforced with cellulose micro/nanofibrils: study of physical, optical, surface, barrier and mechanical properties. Nord. Pulp Pap. Res. J. 1–19. https://doi.org/10.1515/npprj-2022-0006.
Mascarenhas, A.R.P., Scatolino, M.V., Dias, M.C., Martins, M.A., Melo, R.R., Damásio, R. A.P., Mendonça, M.C., Tonoli, G.H.D., 2022b. Fibers pre-treatments with sodium silicate affect the properties of suspensions, films, and quality index of cellulose micro/nanofibrils. Nord. Pulp Pap. Res. J., Ahead Print. 1–19. https://doi.org/10.1515/npprj-2022-0037.
Meiszterics, A., Rosta, L., Peterlik, H., Rohonczy, J., Kubuki, S., Henits, P., Sinkó, K., 2010. Structural characterization of gel-derived calcium silicate systems. J. Phys. Chem. 114, 10403–10411. https://doi.org/10.1021/jp1053502.
Mejia-Ballesteros, J.E., Rodier, L., Filomeno, R., Savastano Jr, H., Fiorelli, J., Rojas, M.F., 2021. Influence of the fiber treatment and matrix modification on the durability of eucalyptus fiber reinforced composites. Cem. Concr. Compos. 124, 104280 https://doi.org/10.1016/j.cemconcomp.2021.104280.
Mendonça, M., Dias, M.C., Martins, C.C.N., Durães, A.F.S., Damásio, R.A.P., Tonoli, G.H. D., 2022. Alkaline pretreatment facilitate mechanical fibrillation of unbleached cellulose pulps for obtaining of cellulose micro/nanofibrils (MFC). J. Nat. Fibers 1–17. https://doi.org/10.1080/15440478.2022.2092252. Ahead–Print.
Mielonen, K., Geydt, P., Österberg, M., Johanasson, L.S., Backfolk, K., 2015. Inkjet ink spreading on polyelectrolyte multilayers deposited on pigment coated paper. J. Colloid Interface Sci. 438, 179–190. https://doi.org/10.1016/j.jcis.2014.09.077.
Miller, S.A., 2020. Five misperceptions surrounding the environmental impacts of single-use plastic. Environ. Sci. Technol. 54, 14143–14151. https://doi.org/10.1021/acs.est.0c05295?ref=pdf.
Mirmehdi, S., Oliveira, M.L.C., Hein, P.R.G., Dias, M.V., Sarantópoulos, C.I.G.L., Tonoli, G.H.D., 2018a. Spraying cellulose nanofibrils for improvement of tensile and barrier properties of writing printing WeP. Paper. J. Wood Chem. Technol. 1–13. https://doi.org/10.1080/02773813.2018.1432656.
Mirmehdi, S., Hein, P.R.G., Sarantópoulos, C.I.G.L., Dias, M.V., Tonoli, G.H.D., 2018b. Cellulose nanofibrils/nanoclay hybrid composite as a paper coating: Effects of spray time, nanoclay content and corona discharge on barrier and mechanical properties of the coated papers. Food Packag. Shelf Life 15, 87–94. https://doi.org/10.1016/j.fpsl.2017.11.007.
Mnasri, A., Dhaouadi, H., Khiari, R., Halila, S., Mauret, E., 2022. Effects of deep eutectic solvents on cellulosic fibres and paper properties: Green "chemical" refining. Carbohydr. Polym. 292, 119606 https://doi.org/10.1016/j.carbpol.2022.119606.
Morais, F.P., Carta, A.M.M.S., Amaral, M.E., Curto, J.M.R., 2021. Micro/nano-fibrillated cellulose (MFC/NFC) fibers as an additive to maximize eucalyptus fibers on tissue paper production. Cellulose 28, 6587–6605. https://doi.org/10.1007/s10570-021-03912-9.
Oliveira, M.L.C., Mirmehdi, S., Scatolino, M.V., Guimarães Júnior, M., Sanadi, A.R., Damásio, R.A.P., Tonoli, G.H.D., 2022. Effect of overlapping cellulose nanofibrils and nanoclay layers on mechanical and barrier properties of spray-coated papers. Cellulose 29, 1097–1113. https://doi.org/10.1007/s10570-021-04350-3.
Otto, S., Strenger, M., Maier-Nöth, A., Schimid, M., 2021. Food packaging and sustainability – consumer perception vs. correlated scientific facts.: A review. J. Clean. Prod. 298, 126733 https://doi.org/10.1016/j.jclepro.2021.126733.
Ozcan, A., Kandirmaz, E.A., 2020. Natural ink production and printability studies for smart food packaging. Color Res. Appl. 45, 495–502. https://doi.org/10.1002/col.22488.
Ozcan, A., Sonmez, S., Tutak, D., 2021. Effect of coating pigment type on paper printability with water-based inks. J. Coat. Technol. Res., Print. 1–9. https://doi.org/10.1007/s11998-021-00593-8.
Özgenç, O., Durmaz, S., Boyaci, I.H., Eksi-Kocak, H., 2017. Determination of chemical changes in heat-treated wood using ATR-FTIR and FT Raman spectrometry. Spectrochim. Acta Part A: Mol. Biomol. Spectrosc. 171, 395–400. https://doi.org/10.1016/j.saa.2016.08.026.
Patel, V.R., Agrawal, Y.K., 2011. Nanosuspension: An approach to enhance solubility of drugs. J. Adv. Pharm. Technol. Res. 2, 81–87 https://dx.doi.org/10.4103 %2F2231-4040.82950.
Pawlowski, L., 2009. Suspension and solution thermal spray coatings. Surf. Coat. Technol. 203, 2807–2829. https://doi.org/10.1016/j.surfcoat.2009.03.005.
Predoi, D., Iconaru, S.L., Predoi, M.V., Motelica-Heino, M., Buton, N., Megier, C., 2020. Obtaining and characterizing thin layers of magnesium doped hydroxyapatite by dip coating procedure. Coatings 10, 510. https://doi.org/10.3390/coatings10060510.
Puertas, F., Fernández-Jiménez, A., Blanco-Varela, M.T., 2004. Pore solution in alkali-activated slag cement pastes. Relat. Compos. Struct. Calcium Silic. hydrate. Cem. Concr. Res. 34, 139–148. https://doi.org/10.1016/S0008-8846(03)00254-0.
Rastogi, V.K., Samyn, P., 2015. Bio-Based coatings for paper applications. Coatings 5, 887–930. https://doi.org/10.3390/coatings5040887.
Ray, S., Dash, J., Devi, N., Sasmal, S., Pesala, B., 2018. Comparative study of hydration kinetics of cement and tricalcium silicate using terahertz spectroscopy and density functional theory simulations. J. Infrared, Millim., Terahertz Waves 39, 651–666. https://doi.org/10.1007/s10762-018-0501-7.
Roig, F., Dantras, E., Dandurand, J., Lacabanne, C., 2011. Influence of hydrogen bonds on glass transition and dielectric relaxations of cellulose. J. Phys. D: Appl. Phys. 44, 045403 https://doi.org/10.1088/0022-3727/44/4/045403.
Rol, F., Belgacem, M.N., Gandini, A., Bras, J., 2019. Recent advances in surface-modified cellulose nanofibrils. Prog. Polym. Sci. 88, 241–264. https://doi.org/10.1016/j.progpolymsci.2018.09.002.
Rotermel, M.V., Samigullina, R.F., Ivanova, I.V., Baklanova, I.V., Krasnenko, T.I., 2021. Synthesis of the synthesis of the $Zn_{1.9}$ $Cu_{0.1}$ SiO_4 pigment via the sol–gel and coprecipitation methods. J. Sol. -Gel Sci. Technol. 100, 404–413. https://doi.org/10.1007/s10971-021-05648-1.
Rueden, C.T., Schindelin, J., Hiner, M.C., Dezonia, B.E., Walter, A.E., Arena, E.T., Eliceiri, K.W., 2017. ImageJ2: ImageJ for the next generation of scientific image data. BMC Bioinforma. 18, 529. https://doi.org/10.1186/s12859-017-1934-z.
Sadek, D.M., El-Attar, M.M., Ali, H.A., 2016. Reusing of marble and granite powders in self-compacting concrete for sustainable development. J. Clean. Prod. 121, 19–32. https://doi.org/10.1016/j.jclepro.2016.02.044.
Saedi, A., Jamshidi-Zanjani, A., Darban, A.K., 2021b. A review of additives used in the cemented paste tailings: environmental aspects and application. J. Environ. Manag. 289, 112501 https://doi.org/10.1016/j.jenvman.2021.112501.
Saedi, S., Garcia, C.V., Kim, J.T., Shin, G.H., 2021a. Physical and chemical modifications of cellulose fibers for food packaging applications. Cellulose 28, 8877–8897. https://doi.org/10.1007/s10570-021-04086-0.
Salmén, L., Larsson, P.A., 2018. On the origin of sorption hysteresis in cellulosic materials. Carbohydr. Polym. 182, 15–20. https://doi.org/10.1016/j.carbpol.2017.11.005.
SCAN Standard, 2000. SCAN-C 62:00, Chemical pulp – Water retention value.
Scatolino, M.V., Bufalino, L., Dias, M.C., Mendes, L.M., Silva, M.S., Tonoli, G.H.D., Souza, T.M., Alves Junior, F.T.A., 2022. Copaiba oil and vegetal tannin as functionalizing agents for açai nanofibril films: valorization of forest wastes from Amazonia. Environmental Science and Pollution Research. in press,, pp. 1–16.
Selvam, N.C.S., Kumar, R.T., Kennedy, L.J., Vijaya, J.J., 2011. Comparative study of microwave and conventional methods for the preparation and optical properties of novel MgO-micro and nano-structures. J. Alloy. Compd. 509, 9809–9815. https://doi.org/10.1016/j.jallcom.2011.08.032.
Shen, Z., Rajabi-Abhari, A., Oh, K., Yang, G., Youn, H.J., Lee, H.L., 2021. Improving the barrier properties of packaging paper by polyvinyl alcohol based polymer coating—effect of the base paper and nanoclay. Polymers 13, 1334. https://doi.org/10.3390/polym13081334.
Shenoy, R., Shetty, P., 2022. New eco-friendly coating formulations for recycled paperboards: effect on print quality and ink volume consumption. Prog. Color., Color. Coat. 15, 175–189. https://doi.org/10.30509/pccc.2021.166804.1110.
Silva, L.C.E., Cassago, A., Batirrola, L.C., Gonçalves, M.C., Portugal, R.V., 2020. Specimen preparation optimization for size and morphology characterization of nanocellulose by TEM. Cellulose 27, 5435–5444. https://doi.org/10.1007/s10570-020-03116-7.
Silva, L.E., Santos, A.A., Torres, L., McCaffrey, Z., Klamczynski, A., Glenn, G., Sena Neto, A.R., Wood, D., Williams, T., Orts, W., Damásio, R.A.P., Tonoli, G.H.D., 2021. Redispersion and structural change evaluation of dried microfibrillated cellulose. Carbohydr. Polym. 252, 117165 https://doi.org/10.1016/j.carbpol.2020.117165.
Spinthaki, A., Petratos, G., Matheis, J., Hater, W., Demadis, K.D., 2018. The precipitation of "magnesium silicate" under geothermal stresses. Form. Charact. Geotherm. 74, 172–180. https://doi.org/10.1016/j.geothermics.2018.03.001.
Tang, S., Wang, Y., Geng, Z., Xu, X., Yu, W., Hubao, A., Chen, J., 2021. Structure, fractality, mechanics and durability of calcium silicate hydrates. Fractal Fract. 5, 47. https://doi.org/10.3390/fractalfract5020047.
Tanzadeh, R., Shafabakhsh, G., 2020. Surface free energy and adhesion energy evaluation of modified bitumen with recycled carbon black (micro-nano. from gases and petrochemical waste. Constr. Build. Mater. 245, 118361 https://doi.org/10.1016/j.conbuildmat.2020.118361.
TAPPI Standard, 2002. T 211 om-02, Ash in wood, pulp, paper and paperboard: combustion at 525 °C.

TAPPI Standard, 2014. T 458 cm-14, Surface wettability of paper (angle of contact method).

Thébault, M., Kandelbauer, A., Müller, U., Zikulnig-Rusch, E., Lammer, H., 2017. Factors influencing the processing and technological properties of laminates based on phenolic resin impregnated papers. Eur. J. Wood Wood Prod. 75, 785–806. https://doi.org/10.1007/s00107-017-1205-8.

Tonoli, G.H.D., Rodrigues Filho, U.P., Savastano Júnior, H., Bras, J., Belgacem, M.N., Lahr, F.A.R., 2009. Cellulose modified fibres in cement-based composites. Compos. Part A: Appl. Sci. Manuf. 40, 2046–2053. https://doi.org/10.1016/j.compositesa.2009.09.016.

Tonoli, G.H.D., Holtman, K., Silva, L.E., Wood, D., Torres, L., Williams, T., Oliveira, J.E., Fonseca, A.S., Klamczynski, A., Glenn, G., Orts, W., 2021. Changes on structural characteristics of cellulose pulp fiber incubated for different times in anaerobic digestate. Cerne 27, e102647. https://doi.org/10.1590/01047760202127012647.

Tsai, C.F., Hung, C.H., Kuo, C.N., Chen, C.Y., Peng, Y.N., Shie, M.Y., 2019. Improved bioactivity of 3D printed porous titanium alloy scaffold with chitosan/magnesium-calcium silicate composite for orthopaedic applications. Materials 12, 203. https://doi.org/10.3390/ma12020203.

Tyagi, P., Salem, K.S., Hubbe, M.A., Pal, L., 2021. Advances in barrier coatings and film technologies for achieving sustainable packaging of food products – a review. Trends Food Sci. Technol. 115, 461–485. https://doi.org/10.1016/j.tifs.2021.06.036.

Wang, F.J., Wang, L.Q., Zhang, X.C., Ma, S.F., Zhao, Z.C., 2022. Study on the barrier properties and antibacterial properties of cellulose-based multilayer coated paperboard used for fast food packaging. Food Biosci. 46, 101398 https://doi.org/10.1016/j.fbio.2021.101398.

Wang, J., Gardner, D.J., Stark, N.M., Bousfield, D.W., Tajvidi, M., Cai, Z., 2018. Moisture and oxygen barrier properties of cellulose nanomaterial-based films. ACS Sustain. Chem. Eng. 6, 49–70. https://doi.org/10.1021/acssuschemeng.7b03523.

Wang, L., Chen, L., Cho, D.W., Tsang, D.C.W., Yang, J., Hou, D., Baek, K., Kua, H.W., Poon, C.S., 2019. Novel synergy of Sci-rich minerals and reactive Mg. for stabilization/solidification of contaminated sediment. J. Hazard. Mater. 365, 695–706. https://doi.org/10.1016/j.jhazmat.2018.11.067.

Wang, L., Chen, C., Wang, J., Gardner, D.J., Tajvidi, M., 2020. Cellulose nanofibrils versus cellulose nanocrystals: comparison of performance in flexible multilayer films for packaging applications. Food Packag. Shelf Life 23, 100464. https://doi.org/10.1016/j.fpsl.2020.100464.

Wang, Y., Wang, G., Wang, H., Liang, C., Cai, W., Xhang, L., 2010. Chemical-template synthesis of micro/nanoscale magnesium silicate hollow spheres for waste-water treatment. Chem. A Eur. J. 15, 3497–3503. https://doi.org/10.1002/chem.200902799.

Wohlert, M., Benselfelt, T., Wagberg, L., Furó, I., Berglund, L.A., Wohlert, J., 2022. Cellulose and the role of hydrogen bonds: not in charge of everything. Cellulose 29, 1–23. https://doi.org/10.1016/j.carbpol.2017.11.005.

Xu, K., Deng, J., Lin, R., Zhang, H., Ke, Q., Huang, C., 2020. Surface fibrillation of para-aramid nonwoven as a multi-functional air filter with ultralow pressure drop. J. Mater. Chem. A 1–13. https://doi.org/10.1039/D0TA07886G.

Yongabi, D., Khorshid, M., Gennaro, A., Jooken, S., Duwé, S., Deschaume, O., Losada-Pérez, P., Dedecker, P., Bartic, C., Wübbernhorst, M., Wagner, P., 2020. QCM-D study of time-resolved cell adhesion and detachment: effect of surface free energy on eukaryotes and prokaryotes. ACS Applied Materials Interfaces 12, 18258–18272 ttps://dx.doi.org/10.1021/acsami.0c00353.

Yu, Z., Dhital, R., Wang, W., Sun, L., Zeng, W., Mustapha, A., Lin, M., 2019. Development of multifunctional nanocomposites containing cellulose nanofibrils and soy proteins as food packaging materials. Food Packag. Shelf Life 21, 100366. https://doi.org/10.1016/j.fpsl.2019.100366.

Zhang, K., Zhang, Y., Yan, D., Zhang, C., Nie, S., 2018b. Enzyme-assisted mechanical production of cellulose nanofibrils: thermal stability. Cellulose 25, 5049–5061. https://doi.org/10.1007/s10570-018-1928-7.

Zhang, T., Zou, J., Wang, B., Wu, Z., Jia, Y., Cheeseman, C.R., 2018b. Characterization of magnesium silicate hydrate (MSH) gel formed by reacting MgO and silica fume. Materials 11, 909. https://doi.org/10.3390/ma11060909.

Zhao, T., Jiang, L., 2018. Contact angle measurement of natural materials. Colloids Surf. B: Biointerfaces 161, 324–330. https://doi.org/10.1016/j.colsurfb.2017.10.056.

Zhao, Z., Li, Z., Cui, P., Li, S., Kong, L., 2015. Adsorption of basic brown and chrysophenine from water solution by magnesium silicate gel. J. Chem. 2015, 1–7. https://doi.org/10.1155/2015/374190.

Zołek-Tryznowska, Z., Kałuza, A., 2021. The influence of starch origin on the properties of starch films: packaging performance. Materials 14, 1146. https://doi.org/10.3390/ma14051146.

Zołek-Tryznowska, Z., Prica, M., Pavlovic, Z., Cveticanin, Annusik, T., 2020. The influence of aging on surface free energy of corona treated packaging films. Polym. Test. 89, 106629 https://doi.org/10.1016/j.polymertesting.2020.106629.